

1 **Assessment of evolving TRMM-based multi-satellite real-time precipitation**
2 **estimation methods and their impacts on hydrologic prediction in a high**
3 **latitude basin**

4
5 Bin Yong^{a,b}, Yang Hong^{b*}, Li-Liang Ren^a, Jonathan J. Gourley^c, George J. Huffman^d,

6 Xi Chen^a, Wen Wang^a, Sadiq I. Khan^b

7
8 ^a*State Key Laboratory of Hydrology-Water Resources and Hydraulic Engineering, Hohai*
9 *University, Nanjing 210098, China*

10 ^b*School of Civil Engineering and Environmental Sciences, University of Oklahoma, Norman,*
11 *OK 73019, USA*

12 ^c*NOAA/National Severe Storm Laboratory, Norman, OK 73072*

13 ^d*Science Systems and Applications, Inc., and Laboratory for Atmospheres, NASA Goddard Space*
14 *Flight Center, Greenbelt, Maryland*

15 Submitted to *Journal of Geophysical Research-Atmosphere*

16
17 *Corresponding author.

18 Dr. Yang Hong

19 *School of Civil Engineering and Environmental Sciences, the University of Oklahoma*

20 *Hydrometeorology and Remote Sensing Laboratory and Atmospheric Radar Research Center,*

21 *National Weather Center 4610 Suite*

22 *Norman, OK 73072 USA*

23 *Email: yanghong@ou.edu*

24 **Abstract**

25 [1] The real-time availability of satellite-derived precipitation estimates provides hydrologists
26 an opportunity to improve current hydrologic prediction capability for medium to large river
27 basins. Due to the availability of new satellite data and upgrades to the precipitation algorithms,
28 the Tropical Rainfall Measuring Mission (TRMM) Multi-satellite Precipitation Analysis real-time
29 estimates (TMPA-RT) have been undergoing several important revisions over the past ten years.
30 In this study, the changes of the relative accuracy and hydrologic potential of TMPA-RT
31 estimates over its three major evolving periods were evaluated and inter-compared at daily,
32 monthly and seasonal scales in the high-latitude Laohahe basin in China. Assessment results show
33 that the performance of TMPA-RT in terms of precipitation estimation and streamflow simulation
34 was significantly improved after 3 February 2005. Overestimation during winter months was
35 noteworthy and consistent, which is suggested to be a consequence from interference of snow
36 cover to the passive microwave retrievals. Rainfall estimated by the new version 6 of TMPA-RT
37 starting from 1 October 2008 to present has higher correlations with independent gauge
38 observations and tends to perform better in detecting rain compared to the prior periods, although
39 it suffers larger mean error and relative bias. After a simple bias correction, this latest dataset of
40 TMPA-RT exhibited the best capability in capturing hydrologic response among the three tested
41 periods. In summary, this study demonstrated that there is an increasing potential in the use of
42 TMPA-RT in hydrologic streamflow simulations over its three algorithm upgrade periods, but
43 still with significant challenges during the winter snowing events.

44

45

46

47 **1. Introduction**

48 [2] Precipitation is fundamental to life on Earth, and it is among the most important factors in
49 energy and mass fluxes that dominate the weather, climate, hydrology, and ecological systems.
50 Therefore, precipitation measurements offer essential information in understanding the balance of
51 the global energy and water cycle exchange that drives most hydrologic models and has direct
52 impacts on the planetary circulation of the atmosphere [*Sorooshian, 2004; Elizabeth et al., 2007*].
53 However, accurately measuring precipitation at regional or global scales has been a challenging
54 task due to its high small-scale variability in space and time. Conventional rain gauge and
55 meteorological radar networks have their own limitations because their distributions are often
56 sparse and data availability in remote regions and in complex terrain is rather limited [*Griffith et*
57 *al., 1978; Simpson et al., 1996; Astin et al., 1997; Vicente et al., 1998; Huffman et al., 2001;*
58 *Margulis et al., 2001; Maddox et al., 2002; Steiner et al., 2003*]. Thus, satellite-based
59 precipitation estimates play an important role in detecting rainfall distribution and have been
60 complementary to the ground-based rain gauge and radar measurements. Since the launch of the
61 Tropical Rainfall Measuring Mission [TRMM; *Simpson et al., 1988 and Kummerow et al., 2000*]
62 in 1997, there has been a growing number of real-time and quasi-global satellite precipitation
63 products [*Sorooshian et al., 2000; Joyce et al., 2004; Hong et al., 2004; Turk and Miller, 2005;*
64 *Huffman et al., 2007; Kubota et al., 2007*] for a variety of scientific uses and natural hazard
65 detection and warning, such as flood forecasting, drought assistance, landslide detection, and
66 water quality monitoring. The planned Global Precipitation Measurement (GPM) mission with an
67 approaching launch date of 14 February 2014 [*Tapiador et al., 2012*], which will use an
68 international constellation of microwave sensors, is anticipated to provide more accurate global
69 precipitation products so as to improve our scientific understanding of the Earth system from

70 space [*Smith et al., 2006; Hou, 2008*]. As a prelude to GPM, the current operational TRMM
71 Multi-satellite Precipitation Analysis (TMPA) is intended to provide the best estimates of
72 quasi-global precipitation [*Huffman et al., 2007*]. The TMPA merged data collected by two
73 different types of satellite sensors: low-Earth orbiting passive microwave (PMW) data, which
74 have a direct physical connection to the hydrometeor profiles but sparse sampling of the
75 time-space occurrence of precipitation, and geostationary infrared (IR) data with excellent
76 space-time coverage (approximately 30 min/4×4 km), but indirect physical relations with
77 precipitation. The standard TMPA products include real time (3B42 RT, hereafter referred to as
78 TMPA-RT) and post-real time research products (3B42 V6, hereafter referred to as TMPA-V6),
79 and both versions of the TMPA products have been provided for a sufficiently long time that
80 researchers have had the chances to develop and start reporting on various applications and
81 validation studies that employ one or both versions [*Huffman et al., 2010*].

82 [3] Many prior studies have reported on the improvement of the TMPA-V6 products over
83 TMPA-RT products through bias correction using monthly rain gauge accumulations [e.g., *Tian*
84 *et al., 2007; Su et al., 2008; Li et al., 2009; Dinku et al., 2010; Gourley et al., 2010; Hirpa et al.,*
85 *2010; Tobin and Bennett, 2010; Behrangi et al., 2011; Betew and Gebremichael, 2011; Yong et*
86 *al., 2010; Su et al., 2011*]. However, it is the near real-time availability of the TMPA-RT products
87 and high spatial (0.25°×0.25°) and temporal (3h) resolution that has made them very attractive to
88 the water resources community, especially in developing countries, in order to provide hydrologic
89 predictions from which actions can be taken on medium to large river basins. Presently,
90 TMPA-RT products have been widely utilized in a variety of research and operational
91 applications [e.g., *Gottschalck et al., 2005; Li et al., 2009; Yong et al., 2010; Tobin and Bennett,*
92 *2010; Behrangi et al., 2011; Khan et al., 2011; Romilly and Gebremichael, 2011; Su et al., 2011;*

93 *Wang et al.*, 2011]. For example, currently the global real-time flood monitoring system
94 developed by NASA TRMM group [<http://trmm.gsfc.nasa.gov/>; *Hong et al.*, 2007; *Wang et al.*,
95 2011; *Wu et al.*, 2012] has demonstrated the initial capability of using satellite-derived
96 precipitation data as forcing for global river forecast models.

97 [4] During the course of TMPA-RT development, precipitation estimates from new sensors on
98 various satellites were integrated and thus the real-time algorithm has undergone several updates.
99 Table 1 summarizes all precipitation-sensing microwave satellites/sensors that were introduced
100 into the TMPA processing at different historical periods. Generally speaking, the evolution of
101 TMPA-RT can be separated into the following three main development periods: 29 January 2002
102 to 3 February 2005 (Period I), 3 February 2005 to 1 October 2008 (Period II), and 1 October 2008
103 to present (Period III). Specific details regarding the sensors used, nominal coverage, and
104 algorithmic changes are provided in Appendix A.

105 **Insert Table 1 here**

106 [5] Given the dynamical evolution of the TMPA-RT algorithm by the Appendix A, a thorough
107 understanding to the above-mentioned major upgrades is critical to physically analyzing the
108 changes of data accuracy and hydrologic potential of the real-time TMPA products across the
109 three different developing periods. Many efforts have been made in prior studies to evaluate the
110 hydrologic utility of TMPA-RT for different basins throughout the globe [e.g., *Li et al.*, 2009;
111 *Dinku et al.*, 2010; *Hirpa et al.*, 2010; *Betew and Gebremichael*, 2011; *Khan et al.*, 2011; *Su et al.*,
112 2011]. Yet, their study areas are rarely located at the high latitude bands beyond the current
113 TMI/PR orbiting regions. Below, we highlight a number of questions about the TMPA-RT
114 algorithm evolution with the intention of addressing them in this study:

115 (1) Have the TMPA-RT estimates been significantly improved over the three major evolution
116 periods?

117 (2) TMI and TCI, the calibrators of TMPA-RT, provide coverage from 40°N-S. Thus, do the
118 data of TMPA-RT that cover higher latitude bands beyond 40° suffer from large bias, especially in
119 basins with snow-covered land surfaces?

120 (3) Are the latest TMPA-RT products (i.e., 3B42RT-Version6) much more similar to the
121 gauge-adjusted TMPA-V6 estimates than the previous two periods as suggested by the developers,
122 particularly in high-latitude basins?

123 (4) Finally, how did changes in input data and algorithm design for TMPA-RT over the three
124 different periods impact hydrologic prediction skill?

125 [6] *Yong et al. [2010]* evaluated the data accuracy and hydrological potential of TMPA-RT and
126 TMPA-V6 in the Laohahe Basin, China within the TMPA latitude band (50°NS) but beyond the
127 latitude band of the TMPA calibrator (40°N-S). In this study, we extend the work of *Yong et al.*
128 [2010] by specifically addressing the above questions through evaluation of TMPA-RT
129 precipitation products using independent gauge reports and examination of TMPA-RT estimates
130 on hydrologic simulation using the three-layer Variable Infiltration Capacity (VIC-3L) Model
131 [*Liang et al., 1994, 1996*]. Section 2 describes the Laohahe basin, the datasets used, and the
132 statistics used to evaluate TMPA precipitation estimates and resulting hydrologic simulations.
133 The precipitation evaluation is divided into daily, monthly, and seasonal analyses in section 3;
134 this section also evaluates the similarity between TMPA-RT to TMPA-V6. The impact of the
135 algorithmic changes on hydrologic simulation is evaluated in section 4, and the paper is closed in
136 section 5 with conclusions and future recommendations.

137 **2. Study Basin, Observed Data and Methodology**

138 [7] The Laohahe basin, of which a detailed description is provided in *Yong et al.* [2010], is
139 located within the Chinese typical arid and semi-arid regions. Accurate precipitation estimates at
140 high spatio-temporal scale is of particular importance for such drought-prone basins with
141 heterogeneous distributions of surface water resources. Compared to other basins in the northern
142 part of China, the Laohahe basin has a remarkably dense observation network that can offer
143 detailed ground verification for the satellite-derived precipitation estimates (Figure 1). There are
144 52 rain gauges evenly distributed within this 18,112 km² basin and a streamflow station of
145 Xinlongpo located at the watershed outlet to record observations of daily precipitation and
146 streamflow continuously from January 1990 to September 2010. Both the China Meteorological
147 Administration (CMA) and the Chinese Ministry of Water Resources (CMWR) operate all rain
148 gauge networks over mainland China. In practice, the local workers record the precipitation using
149 two approaches (i.e., tipping-bucket raingauge and manual traditional ombrometer). Then these
150 two types of recorded data are crosschecked and the final errors have to be controlled within 4%
151 for daily rainfall observation according to the ministerial standard. Hence, the Laohahe basin
152 gauge network is of high quality and is independent from what *Huffman et al.* [2007] used for the
153 gauge correction of TMPA post-real-time products. With respect to snow observations, they
154 introduced a known volume of warm water to thaw the snow in the standard vessel. So the liquid
155 equivalency of the snow is computed as the total water volume minus the input warm water
156 volume. The observers make a particular mark after the snow water equivalent digit in order to
157 distinguish snow or rainfall as the precipitation type. Such manual but effective recording
158 techniques can ensure the data quality and information of observed snow for our study. Ultimately,
159 these precipitation data will be collected and edited in the Chinese Hydrology Almanac at the end
160 of every year.

161 **Insert Figure 1 here**

162 [8] Daily maximum and minimum temperature and daily average wind speed from 1990 to
163 2010 were gathered from four meteorological stations to force the hydrologic model (see Figure.
164 1). Other data sources such as a digital elevation model (DEM), soil surveys, and vegetation,
165 which are needed to run the VIC-3L model, were taken from *Yong et al.* [2010]. The grid mesh
166 size of the hydrologic model used in this study is $\frac{1^\circ}{16} \times \frac{1^\circ}{16}$. To quantify the accuracy of
167 satellite-derived precipitation estimates, we used three types of statistical indices including
168 Pearson linear correlation coefficient (CC), mean error (ME), root mean squared error (RMSE),
169 relative bias (BIAS), and contingency table-based detection of rainy events (i.e., probability of
170 detection (POD), false alarm rate (FAR), and critical success index (CSI)). In addition,
171 Nash-Sutcliffe Coefficient of Efficiency (NSCE) was used to assess the hydrologic model fit
172 between simulated and observed streamflow. The interested reader can refer to all above
173 statistical indices for their corresponding formulae and meaning in Table 1 in *Yong et al.* [2010].

174 **3. Evaluation and Comparison of Satellite Precipitation Estimates**

175 [9] Our evaluation and comparison were performed over three domains including two selected
176 $0.25^\circ \times 0.25^\circ$ grids (hereafter labeled as “Grid0501” and “Grid0401”, see Figure 1) corresponding
177 to TRMM pixel resolution as well as the basin-averaged analysis (hereafter referred to as “Basin
178 Average”). The two, nested grid locations were chosen because they contain 4-5 rain gauges
179 within them and provide an analysis at the fine, TRMM pixel scale. Furthermore, there are
180 significant differences in terrain and land cover between these two grids though they are adjacent
181 to each other. Almost 80% of Grid0401 is at high elevation (>1000 m) with evergreen broadleaf
182 or coniferous trees, while most regions within Grid0501 are considered flat croplands and
183 lowlands (elevations < 1000 m) and are predominately covered by sparse grassland and shrubs.

184 The rain gauge accumulations from each gauge are averaged within each TRMM pixel so that
185 they can be compared to the TMPA estimates. The objective aims to investigate the evolution of
186 the performance of TMPA-RT during the three periods at daily, monthly, and seasonal time scale.
187 Algorithm skill in estimating rainfall amounts is compared to that obtained with TMPA-V6 in
188 order to assess whether TMPA-RT is approaching the skill of TMPA-V6 following the critical
189 algorithm updates. Considering both the major upgrade periods of TMPA-RT and the time span
190 of available observation data in the Laohahe basin, we separated the comparison periods of this
191 study into three parts: Period I (1 February 2002 – 1 January 2005), Period II (1 February 2005 –
192 30 September 2008), and Period III (1 October 2008 – 30 September 2010). The different sensors,
193 data inputs, and algorithm changes during these three time periods are summarized in Table 1 and
194 the details are available in the Appendix A.

195 **3.1 Daily Comparison**

196 [10] We start with the evaluation of daily TMPA-RT against averaged rain gauge observations
197 over Grid0501, Grid0401, and Basin Average across Periods I, II, III, respectively (Figure 2 and
198 3). There is a gradually increasing CC between TMPA-RT and observed precipitation from
199 Period I to III for all three domains (Figure 3a). Taking the domain of Basin Average for example,
200 the CC value increases from 0.46 in Period I to 0.75 in Period III (increasing by approximately
201 63%). With respect to ME and BIAS, TMPA-RT during Period III, however, didn't perform as
202 well as expected, and was even worse than Period I for Grid 0501 and Basin Average (Figures 3c
203 and 3e). But, it is worth noting that TMPA-RT exhibits a significant improvement in the skill of
204 detecting rain events. The indices of POD and CSI are substantially increased throughout the
205 three evolving periods (Figure 2 and Figure 3g), while the FAR has an obvious decreasing
206 tendency (Figure 3i). The results suggest that the new algorithm adjustments to
207 3B42RT-Version6 (i.e., TMPA-RT during Period III) do not always reduce the error and bias of

208 the 3B42RT estimates, but they apparently provide higher correlation with gauge observations
209 and better detection for precipitation events in high-latitude basins, which are potentially
210 favorable factors for improving the hydrologic potential of TMPA-RT. On the other hand,
211 statistics describing TMPA-V6 performance don't reflect the same tendencies noted with
212 TMPA-RT over the three periods, though it has relatively low ME and BIAS (see the right
213 column of Figure 3). Lastly, scatterplots in Figure 2 reveal an interesting phenomenon in that
214 TMPA-RT has a slight tendency to overestimate lower rainfall rates and underestimate higher
215 ones, which is a similar finding in an evaluation of GOES-based rainfall estimates from *Vicente et*
216 *al.* [1998].

217 **Insert Figure 2 here**

218 **Insert Figure 3 here**

219 **3.2 Monthly Comparison**

220 [11] To directly assess the skill of the TMPA products in tracking the monthly variation of
221 precipitation over the three tested periods, we compare the time series of TMPA-RT, TMPA-V6,
222 and gauge observations over Grid 0501, Grid 0401, and Basin Average in Figure 4. Similar to the
223 daily results, the purely satellite-derived TMPA-RT demonstrated a relatively poor performance
224 in tracing the monthly variations of precipitation during Period I, while substantial improvements
225 were realized after 2005. This result confirms the assertion of *Huffman et al.*, [2010] that all
226 TMPA-RT datasets produced before 3 February 2005 should not be used. However, at least in
227 this high-latitude study basin, the TMPA-RT estimates after 2005 still overestimate precipitation
228 compared to gauges, especially during the winter and summer months. The BIAS of TMPA-RT
229 during Period III is even larger than that during Period II. But the monthly CC of Period III looks
230 better than the prior two periods. We further analyzed the TMPA-RT estimates for two largest
231 snowfall events in the winter of 2010 and two heavy rainstorms in the summer of 2010 (see

232 Figure 5). TMPA-RT significantly overestimates precipitation during all these extreme weather
233 events. For example, for the snowfall event that occurred on 26th February 2010, TMPA-RT
234 dramatically overestimated gauge observations over the whole basin by approximately 2000%
235 (i.e., 62.24 mm for TMPA-RT versus 2.96 mm by gauges for Basin Average). Similarly, for the
236 largest rainstorm in 2010, the cumulative gauge precipitation from the 23rd to 31st July is
237 70.81mm for Basin Average, while the corresponding estimation of TMPA-RT is 198.81mm,
238 indicating overestimation of 180%. In contrast, precipitation from TMPA-V6 remains in good
239 agreement with gauge precipitation throughout all the periods (see Figure 4 and 5).

240 **Insert Figure 4 here**

241 **Insert Figure 5 here**

242 [12] Next, we selected three statistical indices, CC, ME, and BIAS to illustrate the evolution of
243 monthly error characteristics of TMPA-RT and TMPA-V6. The values of CC improve throughout
244 all three tested periods, while relatively large values of ME and BIAS were still found for Period
245 III (see Figure 6). Above analyses suggest that the incorporation of AMSU-B and AMSR-E on
246 February 2005, which provides more passive microwave data covering high-latitude bands,
247 significantly improved the accuracy of TMPA-RT precipitation estimates. Another important
248 factor might be that the microwave-calibrated IR coefficients were updated every 3hr instead of
249 each pentad, and thus the IR-based scheme for filling PMW coverage gaps was substantially
250 changed at higher latitudes. Relative to the prior two periods, the latest upgrades of TMPA-RT
251 greatly helped it to improve its correlation with observed precipitation and improve the skill of
252 detecting rainy events, but the incorporation of PMW and IR data did little to reduce ME and
253 BIAS. We speculate that the causes for such large bias of the current TMPA-RT version come
254 from two sources: 1) The PMW data for TMPA are first calibrated by the TRMM Combined
255 Instrument (TCI) estimate, which combines data from TMI and PR. However, the coverage of

256 both TMI and PR is limited within the latitude bands between 40°N-S. 2) Likewise, the TMI-TCI
257 used as the climatological monthly calibrator in 3B42RT-Version6 also cannot cover latitude
258 bands beyond 40°. Thus, the IR-based schemes are poorly calibrated for higher latitudes to the
259 passive microwave, especially during the cool season. Therefore, the upgrades to the TMPA
260 algorithm had little impact on ME and BIAS. The monthly TMPA-V6 data didn't reveal any clear
261 trends in error characteristics over the three periods, thus the relatively higher CC and lower ME
262 can mostly be attributed to the monthly gauge adjustments yielding the post-real-time products
263 [Su et al., 2008; Yong et al., 2010].

264 **Insert Figure 6 here**

265 **3.3 Seasonal Comparison**

266 [13] Table 2 lists the statistical summary of seasonal comparisons including spring
267 [March-May (MAM)], summer [June-August (JJA)], autumn [September-November (SON)], and
268 winter [December-February (DJF)]. We also specifically computed the statistics during winter by
269 separating snow vs. rain events in order to assess the impact of precipitation phase on TMPA-RT.
270 Generally, there are strong seasonal variations in the computed statistics during the three tested
271 periods. All evaluations over Grid0501, Grid0401, and Basin Average show higher CC, POD, and
272 CSI and lower FAR in the summer compared to other seasons, while the worst performance
273 occurs in winter. In terms of the first four indicators, all seasons tended to experience better
274 precipitation estimates during the three evolving periods of TMPA-RT. For example, the CC
275 value of Basin Average in summer rises from 0.48 in Period I to 0.68 in Period II, and finally
276 reaches 0.85 in Period III. For random error and bias there are the largest values of ME and
277 RMSE in summer months because both the amount and frequency of precipitation are highest in
278 this season. By analyzing all values of ME, RMSE, and BIAS for different seasons throughout the

279 three different periods, we can conclude that the errors in Period III found in the daily and
280 monthly comparisons (Figure 3 and 6) are primarily attributed to the overestimation of the
281 3B42RT-Version6 algorithm for summer rainstorms. In addition, it is worth noting that the largest
282 relative biases occur in winter in estimating the water equivalent with snowing events. After
283 excluding these snowing days, we found that the CC evidently increased from Period I to III,
284 meanwhile ME, RMSE, and BIAS improved significantly in winter. Moreover, the detection of
285 precipitating events also performs slightly better for rainy days. In general, approximately 45% of
286 the total annual errors come from heavy rainfall events in summer, while the proportion during
287 winter is only 15%.

288 **Insert Table 2 here**

289 [14] To help developers diagnose the impact of snow on TMPA estimates in high-latitude
290 basins, we calculated the number of snowing days, cumulative snow water equivalent, and four
291 representative statistical indices (i.e., CC, ME, RMSE, and BIAS) of TMPA-RT and TMPA-V6
292 vs. Gauge for the winters from 2005 to 2010 in the Laohahe basin (see Table 3). It is notable that
293 TMPA-RT has relatively better cool season performance during the years with the least number
294 of snowing days. For example, the best performance occurred in the winter of 2009, which only
295 has two snowing days and 2.35 mm of snowmelt for the whole basin. In contrast, the worst
296 performance is found in the winter of 2010 with the maximum of snowing days (5 days) and
297 water-equivalent cumulative snowmelt (10.54 mm). The overestimation with TMPA-RT during
298 winter months in the Laohahe basin was especially remarkable and consistent, which might be
299 attributed to two major reasons: 1) The IR-based retrievals with high space-time coverage, but
300 poor correlation with rainfall (or snow water equivalent), are the main inputs of the TMPA system
301 in high-latitude areas. Unfortunately, IR-based estimates with warm-top stratiform cloud systems
302 perform rather poorly during the cold seasons [Vicente *et al.*, 1998; Tian *et al.*, 2007]. 2) As

303 another confounding factor, the snow cover in winter very likely interferes with the PMW-based
304 retrievals [Grody, 1991; Ferraro et al., 1998], such as these two important microwave sensors of
305 AMSR-E and AMSU-B that can cover higher-latitude bands (beyond 40°N-S). In particular, the
306 high frequency channels (89 and 150-GHz) of AMSU-B might detect more scattering associated
307 with precipitation sized ice particles in the winter atmosphere, which indirectly raises its retrieval
308 precipitation rate [Vila et al., 2007]. Thus, the available PMW-based calibrations of IR and the
309 PMW data themselves covering high-latitude regions cannot offer accurate retrievals with snow
310 events. As a result, the TMPA estimates suffer serious bias during the cool seasons.

311 **Insert Table 3 here**

312 **3.4 Detection of Similarity between TMPA-RT and TMPA-V6**

313 [15] Some previous studies have verified that TMPA-V6 showed better performance in
314 hydrologic simulation than TMPA-RT in many basins over the globe [Su et al., 2008; Stisen and
315 Sandholt, 2010; Yong et al., 2010; Betew and Gebremichael, 2011]. Meanwhile, the TMPA
316 producers also suggested that the real-time datasets were made to be similar to the research
317 products as much as possible. Therefore, we specifically address the following question that
318 naturally arises amongst data users: Did the latest upgrades make TMPA-RT closer to TMPA-V6
319 than before? To address this issue, we first plotted the annual statistical indices of TMPA-RT vs.
320 TMPA-V6 over Grid0501, Grid0401, and Basin Average during 2002-2010 (Figure 7). The
321 results of annual statistics show that the TMPA-RT estimates after 2005 generally have higher
322 correlation, lower errors, and better rain detection against TMPA-V6 than before. However,
323 TMPA-RT of Period III doesn't continue the tendency of approaching the skill of TMPA-V6 like
324 that from Period I to Period II. Four statistics (i.e., CC, POD, FAR, and CSI) of Period III show
325 no clear significant improvements compared with Period II. The indices of error and bias (i.e.,

326 ME, RMSE, and BIAS) are even larger than those of Period II.

327 **Insert Figure 7 here**

328 [16] Considering the strong seasonality within satellite-based precipitation estimates, we
329 further investigated the seasonal statistics of TMPA-RT vs. TMPA-V6 for more insightful
330 understanding. Figure 8a and 8c show that there are gradually increasing CC, POD, and CSI
331 between TMPA-RT and TMPA-V6 from Period I to III during the spring and autumn seasons.
332 Interestingly, the values of error and bias (ME, RMSE, and BIAS) and false alarm ratio (FAR)
333 have a significant decreasing tendency for these two seasons, which is different from the annual
334 statistics. However, such variations expected by the TMPA producers were not found in the
335 seasons of summer and winter (Figure 8b and 8d). For instance, the values of ME, RMSE, and
336 BIAS in Period III are higher than those values in Period II during the summer months. For winter,
337 besides similar overestimation of error and bias, the POD values of three domains even show
338 anomalous fluctuations. Therefore, it can be concluded that relative to the prior two periods, the
339 larger bias and error between TMPA-RT and TMPA-V6 during Period III are chiefly attributed to
340 the remarkable overestimation of the TMPA-RT algorithm for the summer rainstorms and the
341 winter snowfall over our high-latitude basin.

342 **Insert Figure 8 here**

343 **4. Evaluation and Comparison of Hydrologic Streamflow Simulations**

344 [17] Up to this point, we have directly evaluated the precipitation estimates from TMPA-RT
345 and TMPA-V6. The purpose of this section is to assess the impacts of the TMPA-RT's upgrades
346 over the three evolving periods from the hydrologic perspective after applying the estimates as
347 forcing to the VIC-3L hydrologic model. The VIC-3L model was calibrated using monthly rain
348 gauge and streamflow observations on the Laohahe basin for the period 1990-1999 by *Yong et al.*,

349 [2010]. Figure 9a shows the monthly series of observed and VIC-simulated streamflow using rain
350 gauge inputs from 1990-2010. The plots of cumulative annual precipitation and streamflow
351 indicate that the annual rainfall of the Laohahe basin hardly changed during the last twenty years
352 (Figure 9b). However, there is a dramatic decreasing tendency with the observed discharge after
353 2000 (Figure 9c). *Yong et al.* [2010] concluded that human activities such as increased water
354 diversions for irrigation, newly built reservoirs and dams, rapid development of water-consuming
355 industries, and growth of local economies have substantially altered the natural hydrologic system.
356 Here, we emphasize that the streamflow after 2000 cannot be used as a standard reference for
357 assessing TMPA's hydrologic potential provided that the model parameters were estimated prior
358 to 2000 due to the tremendous human impacts in this basin. Therefore, as recommended by some
359 previous studies [e.g., *Wang et al.*, 2010; *Yong et al.*, 2010], we adopted the streamflow
360 reconstructed with gauge-observed precipitation input to the hydrologic model as the surrogate
361 for the observed streamflow during 2000-2010 (i.e., reconstruction period) in following
362 hydrologic evaluations.

363 **Insert Figure 9 here**

364 [18] We designed three simulation schemes (i.e., validation, bias-correction, and recalibration)
365 to assess and inter-compare the hydrologic potential of TMPA-RT over the three evolving periods
366 using the reconstructed streamflow as the reference. First, we kept the same calibrated parameters
367 optimized during the calibration period 1990-1999 unchanged and used the $\frac{1}{16}^{\circ} \times \frac{1}{16}^{\circ}$ gridded
368 TMPA-RT and TMPA-V6 data to directly force the VIC-3L model for hydrologic simulation.
369 Figure 10 shows that simulations using TMPA-RT significantly overestimates streamflow in the
370 Laohahe basin mostly due to its unrealistically high precipitation estimates as presented in section
371 3. However, it is worth noting that there is a gradually increasing tendency in the correlation

372 between TMPA-RT-derived and reconstructed streamflow during the three periods. For example,
 373 CC of daily streamflow in Period I is 0.02, while this value rises to 0.24 in Period II and to 0.45 in
 374 Period III. With respect to monthly simulation, the values of CC are -0.11, 0.49, and 0.61 for the
 375 three periods, respectively. On the other hand, TMPA-V6 exhibits very good performance in
 376 simulating the daily and monthly variations of reconstructed streamflow, compared with
 377 TMPA-RT. Moreover, the streamflow driven by TMPA-V6 even agrees with the reconstructed
 378 reference runoff more than the observed streamflow due to the significance of land use changes
 379 and human infrastructure impacts on streamflow in the Laohahe basin. In other words,
 380 satellite-derived precipitation estimates should have greater potential applications in simulating
 381 natural hydrologic processes for typical ungauged basins which experience much lower human
 382 impacts.

383 **Insert Figure 10 here**

384 [19] The hydrologic validation in Figure 10 suggests that there exists a high system bias in the
 385 TMPA-RT estimates for our study basin. We speculate that similar results might be prevailing
 386 with other high-latitude basins. Therefore, next we adopted a simple bias reduction method to
 387 potentially improve streamflow prediction using TMPA-RT at basin scale. In the proposed
 388 approach, we defined a ratio bias correction factor (rr) as:

$$389 \quad rr = \frac{1}{1 + \text{BIA}} \quad (1)$$

390 where the relative bias (BIAS) is defined as following:

$$391 \quad \text{BIAS} = \frac{\sum_{i=1}^n (S_i - G_i)}{\sum_{i=1}^n G_i} \times 100\% \quad (2)$$

392 In (2), S_i is the daily or monthly precipitation of TMPA-RT at the i^{th} time step, G_i is the

393 corresponding gauge precipitation, and n is the number of time steps.

394 [20] Next, the bias correction factor (rr) was applied to the satellite precipitation retrievals
395 (i.e., $rr \times \text{TMPA}$) for each of the three tested periods (rr was 0.5622 for Period I, 0.6038 for
396 Period II, and 0.4918 for Period III). We kept the calibrated model parameters the same and
397 merely replaced the original TMPA-RT estimates with the bias-corrected inputs to drive the
398 VIC-3L hydrologic model. As we anticipated, the simple approach of bias-correction remarkably
399 improved the application of TMPA-RT estimates to streamflow simulation (Figure 11). The
400 TMPA-RT-driven simulation agrees well with the reconstructed streamflow especially after 2005.
401 The best hydrological performance was found in Period III (NSCE of 0.39 and 0.67, CC of 0.63
402 and 0.85 for daily and monthly streamflow prediction, respectively) despite some overestimates
403 during the summer and winter months of 2010. Apparently, it was the higher CC and better
404 rainfall detection skill (POD, FAR, and CSI) of TMPA-RT precipitation with rain gauges during
405 Period III compared to the prior two periods that drastically improved its hydrologic capability.
406 Following the simple procedure of bias-correction, the TMPA-RT was closer to observed
407 precipitation and its potential for capturing the hydrological features of the basin was significantly
408 enhanced for our study basin, though it still cannot achieve the simulation accuracy as in medium-
409 or low-latitude basins (e.g. those reported by *Behrangi et al.* [2011], *Betew and Gebremichael*
410 [2011], and *Su et al.* [2011]).

411 **Insert Figure 11 here**

412 [21] Presently, there is an increasing realization that many hydrologic models are sensitive to
413 the meteorological forcing data, in particular precipitation [*Wilk et al.*, 2006]. If the error
414 characteristics of input precipitation change dramatically, then it is likely that sensitive model
415 parameters, such as soil infiltration parameters and baseflow parameters will need to change
416 accordingly in order to achieve accurate streamflow simulations [*Su et al.*, 2005; *Yong et al.*,

417 2010]. Although bias correction to the forcing data is the preferred approach, these error
418 characteristics may only be known after a given algorithm was implemented and evaluated after a
419 significant passage of time. In other words, the identification of bias may not be readily available
420 for a recently implemented precipitation algorithm or in locations where there are scarce or
421 nonexistent gauge networks. In the third experiment, we recalibrated the sensitive parameters of
422 VIC-3L for the whole period of February 2002 – September 2010 by using the original
423 TMPA-RT precipitation estimates as forcing data. Table 4 lists the calibrated and recalibrated
424 values of the seven sensitive parameters in the VIC-3L model. These parameters are briefly
425 depicted as follows: 1) the infiltration parameter (b) which controls the amount of water that can
426 infiltrate into the soil; 2) the three soil layer thicknesses (d_1, d_2, d_3) which affect the maximum
427 storage available in the soil layers and consequently the water available for transpiration; 3) three
428 baseflow parameters including the maximum velocity of baseflow (D_m), the fraction of maximum
429 baseflow (D_s), and the fraction of maximum soil moisture (W_s), which jointly determine how
430 quickly the water stored in the third layer is withdrawn [Liang *et al.*, 1996; Su *et al.*, 2005].
431 Among them, the most intensive parameters are the infiltration parameter (b) and the second soil
432 layer thicknesses (d_2), which were targeted for intensive calibration/recalibration. Similar to
433 Figure 11, the recalibrated simulations also show that the TMPA-RT after 2005 performed much
434 better than prior periods for hydrologic simulation (see Figure 12). From the values of NSCE and
435 CC, it can be seen that the best performance still occurred in Period III. The recalibrated results
436 suggest again that hydrologic potential of TMPA-RT tends to gradually increase during its three
437 evolving periods. However, the recalibration approach compromised the model's parameterized
438 representation of real-world physical processes. For example, the recalibrated parameter, b , is
439 0.0055 (see Table 4), which almost reaches its minimum value of zero. The other sensitive
440 parameter, d_2 , has an optimized value of 5.7 m that substantially exceeded the upper limit of its

441 normal physical range (0.1-2.0 m). Thus, it can be seen that the bias of TMPA-RT overestimation
442 was mitigated at the cost of comprising the physical representativeness of hydraulic properties of
443 the basin, which seriously alters the basin response under varying wetness conditions. Although
444 the recalibration may not be a physically consistent approach for modeling the hydrologic
445 response of real basins, it certainly helps us to confirm two facts: 1) the errors in simulating
446 streamflow forced by TMPA-RT are mostly due to the unrealistically high precipitation
447 estimation, and 2) there is an increasing hydrologic potential for TMPA-RT in streamflow
448 simulations over its three historic development periods. However, we did not intend to advocate
449 the recalibration as the norm for the satellite QPE-hydrology community, rather than an
450 investigation tactic in this study.

451 **Insert Figure 12 here**

452 **Insert Table 4 here**

453 [22] *Hossain and Lattenmaier [2006]* have argued that a shift in paradigm is needed to properly
454 assess estimates of rainfall from satellite sensors for modeling dynamic hydrologic processes such
455 as the rainfall-runoff transformation and associated energy and moisture fluxes. To better
456 understand how error characteristics of input precipitation affect hydrologic model results, we
457 compared the error propagation of TMPA-RT through VIC-3L rainfall-runoff processes at daily
458 and monthly scale for the above three types of simulation schemes. For NSCE and CC, Table 5
459 shows that the hydrological simulations of scheme 2 (bias-correction) and 3 (recalibration)
460 performed much better than those of scheme 1 (validation). This suggests that both
461 bias-correction and model-parameter adjustment can effectively remove the system bias of
462 TMPA-RT through the VIC-3L model and then improve the hydrologic potential of satellite
463 precipitation in this specific basin. NSCE and CC of TMPA-RT-driven streamflow in scheme 2
464 and 3 exhibit an apparent upward trend over the three tested periods (e.g., NSCE of -1.44, 0.47,

465 and 0.67; CC of 0.18, 0.71, and 0.85 for the monthly streamflow simulation in scheme 2,
466 respectively), which is closely corresponding to the trend in CC between satellite precipitation
467 inputs and observations (e.g., CC of 0.67, 0.80, and 0.91 for the monthly rainfall in scheme 2).
468 Among the three tested periods, the best performance is in Period III. This implies that the
469 upgraded algorithm using climatological monthly calibration that increased the CC, POD, CSI
470 and decreased the FAR between satellite precipitation and gauged observations potentially
471 improved the hydrologic application of TMPA-RT. In terms of BIAS and RMSE, it is shown that
472 the VIC-3L model significantly amplified the errors propagated from original satellite rainfall to
473 the TMPA-RT-driven simulations (refer to the statistics of scheme 1 in Table 5). However,
474 following precipitation bias-correction or model-parameter adjustment, both procedures having
475 the same effect on hydrologic simulation, this situation was remarkably improved. Overall, the
476 results of rainfall-runoff error propagation suggest that the hydrological potential of TMPA-RT
477 tends to become better and better during its evolving periods even in high-latitude regions. The
478 authors argue that such improvements of hydrologic prediction are closely related to the inclusion
479 of new satellite data sources and upgrades to the precipitation algorithms in the TMPA real-time
480 precipitation systems. Additionally, the error in rainfall versus error in runoff presented in Table 5
481 indicates that the hydrologic propagation of satellite rainfall error through the VIC model exhibits
482 a quasi-linear behavior due to the large basin scale (18,112 km²) and longer time scales (daily or
483 monthly) in this study. While previous studies [*Nikolopoulos et al., 2010; Serpetzoglou et al.,*
484 *2010*] have indicated that a strong non-linearity exists in the rainfall-runoff error transformation,
485 those results are generally for hourly flood simulations on smaller-scale basins (<600 km²).
486 Clearly, our results demonstrate that there is a dependence of satellite rainfall error propagation
487 on basin scale.

488 **Insert Table 5 here**

489 **5. Conclusions and Recommendations**

490 [23] In this study, we have evaluated and inter-compared the TMPA-RT precipitation estimates
491 over three major evolution periods at daily, monthly and seasonal time scales using an
492 independent, high-quality rain gauge network in a high-latitude basin in China. Then, we
493 investigated whether the latest updates within Period III made the TMPA-RT data more similar to
494 the gauge-adjusted TMPA-V6 estimates as intended by the algorithm developers. Lastly, we
495 designed three types of streamflow simulation experiments using the VIC-3L model forced by
496 TMPA-RT precipitation estimates in order to explore their hydrologic potential throughout the
497 three evaluation periods. Results drawn from the above analyses may be specific to the Laohahe
498 basin but are likely to be more generally applicable to basins situated in 40°-50° latitude bands;
499 they are summarized as follows:

500 (1) TMPA-RT estimates were least accurate and had the poorest hydrologic performance prior to
501 February 2005 (in Period I), while substantial improvements by use of AMSR-E and
502 AMSU-B data occurred thereafter as the developers have documented. Our results support
503 their recommendation that users of TMPA precipitation should not utilize the real-time
504 datasets before February 2005 for application to or feasibility studies involving hydrologic
505 prediction or other natural hazard studies (e.g., landslides). The post-real-time research
506 products (i.e., TMPA-V6) can be regarded as a reliable substitute to use prior to February
507 2005.

508 (2) Compared to the two prior periods before October 2008 (Periods I and II), the most recent
509 version of TMPA-RT (i.e., 3B42RT-Version6 for Period III in this study) has higher CC,
510 POD, and CSI and lower FAR compared to rain gauge observations. However, it was noted
511 that it also has larger ME, RMSE and BIAS in our study basin. This implied that the latest

512 algorithm upgrades to TMPA-RT tended to increase its correlation with independent rain
513 gauge observations and improve the skill of detecting rainy events, but was not capable of
514 systematically reducing bias. Therefore, caution must be exercised when using the current
515 version 6 of TMPA-RT as inputs for flood forecasting models due to its propensity to
516 overestimate precipitation in higher-latitude basins.

517 (3) The latest upgrades to TMPA-RT during Period III made it more statistically similar to
518 TMPA-V6 than the real-time algorithm running in Period II during the spring and autumn
519 seasons. However, such improved performance anticipated by both the TMPA produced and
520 data users was not found in the summer and winter seasons due to the remarkable
521 overestimation of the current 3B42RT-Version6 algorithm in detecting the summer
522 rainstorms and the winter snowfall over this high-latitude basin.

523 (4) In the present version of TMPA-RT, one of the most serious issues was its notably poor
524 performance (i.e., BIAS > 1000%) during winter months, in particular with snowy events.
525 Apparently, satellite-based precipitation estimates in high latitudes during cold seasons still
526 present significant challenges. Snow-covered surfaces present problems for passive
527 microwave retrievals, which are infrequent at high latitudes. It is also possible that IR-based
528 schemes are poorly calibrated for high-latitude, cool season precipitation estimates.

529 (5) Prior to performing a hydrologic evaluation, streamflow was reconstructed on the Laohahe
530 basin using rain gauge inputs to the calibrated VIC-3L model. This reconstruction step was
531 needed in order to account for the tremendous, unnatural and difficult-to-model reductions to
532 streamflow caused by human impacts after 2000. The first experiment directly input
533 TMPA-RT estimates to the calibrated VIC-3L model and compared simulations with the
534 reconstructed streamflow. Not surprisingly, the TMPA-RT-driven model simulation
535 significantly overestimated the daily and monthly hydrographs for the entire period from

536 2002 to 2010. The second experiment applied a mean bias correction factor to the TMPA-RT
537 estimates for each of the three periods and evaluated them as inputs to the calibrated VIC-3L
538 hydrologic model. In this hydrologic evaluation, the TMPA-RT datasets revealed
539 improvements throughout the three evolving periods. The third, naive experiment
540 incorporated no information about TMPA-RT precipitation bias, which will be the case in
541 basins lacking rain gauge networks, and recalibrated model parameters to the uncorrected,
542 biased TMPA-RT estimates. The hydrologic skill in this latter experiment was essentially the
543 same as that achieved in the second experiment. This indicates the model parameters can be
544 estimated in a manner to effectively remove precipitation bias. However, it is noted that
545 model parameter estimation procedures require a long, multi-year dataset, over which the
546 error characteristics of precipitation might change especially following algorithm updates.
547 Furthermore, the recalibrated parameters didn't always represent the realistic changes of
548 hydraulic properties for real basins. Thus, it is recommended that the best procedure to
549 increase the hydrologic use of TMPA-RT precipitation estimates is to improve their accuracy
550 as much as possible and be cognizant of potential biases.

551 [24] Looking to the future, *Huffman et al.* [2010] suggested that more work is needed to extend
552 TMPA precipitation estimates to higher latitudes and further evaluate the effectiveness of ongoing
553 algorithm upgrades. Compared to the post-real-time research products, TMPA-RT data have
554 attracted the attention of hydrologists who are engaging in studies of flood forecasting and
555 landslide warning over vast regions due to the availability of the data in near-real time over most
556 parts of the globe. We expect the results reported here will both provide the retrieval developers
557 with some valuable references and offer hydrologic users of TMPA-RT data a better
558 understanding of their error characteristics and potential utilization for various operational
559 hydrological applications in high-latitude basins. In summary, this study demonstrated that there

560 is an increasing potential in the use of TMPA-RT in hydrologic streamflow simulations over its
561 evolving periods. But, accurate detection and estimation of precipitation during the winter months
562 (especially for snowing events) is still a challenging task for the satellite-based precipitation
563 estimates. We also note that the evaluation of TMPA-RT across the time history of algorithm
564 development presented herein potentially mixes effects due to varying storm or snowfall
565 characteristics during various years and the changes in the retrieval algorithms themselves.
566 Therefore, a more fair comparison could be accomplished by applying the different algorithmic
567 versions on the same data period, a topic inviting future research. Additionally, the results shown
568 in this study are only from a representative, semi-arid, high-latitude basin in China, so future
569 work should extend to different hydroclimatic basins located in different latitude bands. Moreover,
570 the evaluation framework developed herein can apply to new satellite precipitation products such
571 as the forthcoming 3B42RT Version 7 datasets and future GPM-era products.

572

573 **Appendix A: Major Upgrades of TMPA-RT During Its Three Evolving** 574 **Periods**

575 [25] (1) 29 January 2002 to 3 February 2005 (Period I): Only the observations from two
576 multi-channel passive microwave radiometers, i.e. the TRMM Microwave Imager (TMI) and the
577 Special Sensor Microwave/Imager (SSM/I) on Defense Meteorological Satellite Program (DMSP)
578 platforms, are converted to the merged microwave (3B40RT, or HQ product) precipitation
579 estimates with sensor-specific versions of the Goddard Profiling Algorithm [GPROF; *Kummerow*
580 *et al.*, 1996; *Olson et al.*, 1999]. During this initial period, the microwave HQ product, merged
581 from TMI, PR (precipitation radar, TRMM product 2B31) and SSM/I, was used to calibrate the

582 IR inputs collected from a variety of sensors flying on several geosynchronous Meteorological
583 satellites (refer to the note of Table 1).

584 [26] (2) 3 February 2005 to 1 October 2008 (Period II): Several important upgrades occurred
585 at the beginning of this period for improving the data accuracy and algorithm stability of TMPA.
586 First, Advanced Microwave Scanning Radiometer for Earth Observing System (AMSR-E) on
587 Aqua and 3 Advanced Microwave Sounding Unit-B (AMSU-B) sensors onboard NOAA-series
588 satellites were included into the PMW mosaics to further calibrate the TMPA-RT algorithm,
589 which nearly doubles the typical combined microwave coverage in the latitude band 50°N-S from
590 ~45% to nearly 80% [Huffman *et al.*, 2007]. The polar orbits of AMSR-E and AMSU-B provide
591 broader nominal coverage (see Table 1). Especially, the use of AMSU-B offers an excellent
592 opportunity to reduce the errors associated with the inadequate samples by combining PMW
593 information from three NOAA POES satellites spaced approximately 4 h apart with a spatial
594 resolution of 16 km at nadir and a wider swath than prior SSMI (2200 km) [Vila *et al.*, 2007].
595 However, both AMSU-B and AMSR-E still have some limitations in their retrieval techniques
596 which prevent useful precipitation estimates over many land surfaces or sea ice. Second, the
597 Microwave Humidity Sounder (MHS) on NOAA-18 was incorporated in TMPA-RT to replace
598 the AMSU-B on board NOAA-17 since 27 November 2007. Similar to AMSU-B, the MHS
599 contains 5 channels and maintains almost same algorithm-wise within TMPA-RT. But it was an
600 afternoon sounder with a 1330 equator-crossing time, while the previous AMSU-B on NOAA-17
601 has a morning equator-crossing time of around 1030 local time [Labow *et al.*, 2011]. According to
602 Turk *et al.* [2010], the local crossing time of the AMSU-like sounders did have an impact upon
603 the soil moisture simulated with two land surface models. So presumably they might also affect
604 the hydrologic performance of the TRMM-based precipitation estimation. Third, inter-satellite

605 calibration in the HQ product is climatological, which reduced the real-time computational load
606 and prepared for the eventual decommissioning of TRMM. Finally, the microwave-calibrated IR
607 coefficients are recomputed every three hr to better control unrealistically high estimates
608 associated to unusually cold IR background temperatures (Tb's) but with low rainfall rates, such
609 as with high-level cirrus clouds (ftp://trmmopen.gsfc.nasa.gov/pub/merged/3B4XRT_doc.pdf).

610 [27] (3) 1 October 2008 to present (Period III): The last major upgrades for the TMPA
611 real-time system occurred on 17 February 2009. The datasets of the new Version 6 of the
612 TMPA-RT (hereafter “3B42RT-Version6”; note that this should not to be confused with TMPA
613 post-real time product “3B42V6”) starting from 1 October 2008 were released so as to provide
614 the users a backlog for validation and application activities with the new data. Once the new
615 system is stable, the algorithm developers will seriously consider that the entire data record of
616 TMPA-RT might be reprocessed by the 3B42RT-Version6 scheme. The primary goal of the new
617 design of this algorithm and input data is to enable the real-time TMPA-RT and the post real-time
618 gauge-adjusted products TMPA-V6 systems to be as similar as possible for ensuring consistency
619 between these two datasets [*Huffman et al., 2010*]. One important difference between them is the
620 calibrator of TMPA-V6, TRMM Combined Instrument (TCI) that combines data from both TMI
621 and PR, is not available in real time. Therefore, the developers first determined a matched
622 histogram calibration of TMI to the TCI, computed from 10 years of coincident data to establish
623 the climatology for each calendar month. Then, a climatological monthly calibration of TCI to
624 3B43 V6 (another TRMM product computed at monthly time intervals; not to be confused with
625 aforementioned “3B42V6” and “3B42RT-Version6”) is calculated as a simple ratio on a $1^{\circ} \times 1^{\circ}$
626 grid, aggregated to an overlapping $3^{\circ} \times 3^{\circ}$ template, and using 10 years of data. Finally, the
627 TMI-TCI and TCI-3B43 calibrations are successively applied to the preliminary real-time

628 products to create the 3B42RT-Version 6 products. One of the main purposes of this algorithm
629 upgrade is to reduce the bias of TMPA-RT over land. In addition, the AMSU-B sensor on
630 NOAA-17 was inactive on 12 December 2009 and it was replaced by the MHS sensor on the
631 European Operational Meteorological (MetOp) satellite since 27 March 2009 (Table 1). Later
632 enhancements to the TMPA standard products mainly include improving error quantification and
633 more importantly, extension to higher latitudes.

634

635 [28] **Acknowledgements.** This work was financially supported by the Major Program of National
636 Natural Science Foundation of China (51190090) and the 111 Project (B08048). Also this work is
637 partially sponsored by the National Science Foundation for Young Scientists of China (40901017),
638 the Open Fund of State Key Laboratory of Hydroscience and Engineering (sklhse-2011-A-01),
639 and the Innovative Research Team and Independent Innovation Project of State Key Laboratory
640 of Hydrology-Water Resources and Hydraulic Engineering (2009585412, 2009586512). The first
641 author acknowledges the computational facility provided by Hydrometeorology and Remote
642 Sensing Laboratory and Atmospheric Radar Research Center at University of Oklahoma Research
643 Campus. Additionally, the authors would like to thank three anonymous reviewers who helped to
644 improve the earlier version of this paper. Last but not least, we wish to extend our appreciation to
645 the helpful suggestions of Prof. Fengge Su and Dr. Jiahu Wang for the use of VIC-3L model. The
646 TMPA data used in this study were provided by the NASA/Goddard Space Flight Center's
647 laboratory for Atmospheres and PPS, which develop and compute the TMPA as a contribution to
648 TRMM.

649

650

651 **References**

- 652 Astin, I. (1997), A survey of studies into errors in large scale space-time averages of rainfall,
653 cloud cover, sea surface processes and the Earth's radiation budget as derived from low orbit
654 satellite instruments because of their incomplete temporal and spatial coverage, *Surv.*
655 *Geophys.*, 18, 385-403.
- 656 Behrangi, A., B. Khakbaz, T. C. Jaw, A. AghaKouchak, K. Hsu, and S. Sorooshian (2011),
657 Hydrologic evaluation of satellite precipitation products over a mid-size basin, *J. Hydrol.*, 397,
658 225-237.
- 659 Bitew, M. M., and M. Gebremichael (2011), Evaluation of satellite rainfall products through
660 hydrologic simulation in a fully distributed hydrologic model, *Water Resour. Res.*, 47,
661 W06526, doi:10.1029/2010WR009917.
- 662 Dinku, T., S. J. Connor and P. Seccato (2010), Comparison of CMORPH and TRMM-3B42 over
663 mountainous regions of Africa and South America Satellite, *Applications for Surface*
664 *Hydrology*, edited by F. Hossain and M. Gebremichael, Springer, New York, 193-204.
- 665 Ebert, E. E., J. E. Janowiak, and C. Kidd (2007), Comparison of near-real-time precipitation
666 estimates from satellite observations and numerical models, *Bull. Amer. Meteor. Soc.*, 88,
667 47-64.
- 668 Ferraro, R. R., E. A. Smith, W. Berg, and G. J. Huffman (1998), A screening methodology for
669 passive microwave precipitation retrieval algorithms, *J. Atmos. Sci.*, 55, 1583–1600.
- 670 Gottschalck, J., J. Meng, M. Rodell, and P. Houser (2005), Analysis of Multiple Precipitation
671 Products and Preliminary Assessment of Their Impact on Global Land Data Assimilation
672 System Land Surface States, *J. Hydrometeorol.*, 6(5), 573-598.
- 673 Gourley, J. J., Y. Hong, Z. L. Flamig, L. Li, and J. Wang (2010), Inter-comparison of Rainfall

674 Estimates from Radar, Satellite, Gauge, and Combinations for a Season of Record Rainfall, *J.*
675 *Appl. Meteor. Climatol.*, 49, 437-452.

676 Griffith, G. C., W. L. Woodley, and P. G. Grube (1978), Rain estimation from geosynchronous
677 satellite imagery-visible and infrared studies, *Mon. Weather Rev.*, 106, 1153–1171.

678 Grody, N. C. (1991), Classification of Snow Cover and Precipitation Using the Special Sensor
679 Microwave Imager, *J. Geophys. Res.*, 96(D4), 7423-7435.

680 Hirpa, F. A., M. Gebremichael, and T. Hopson (2010), Evaluation of high resolution satellite
681 precipitation products over very complex terrain in Ethiopia, *J. Appl. Meteor. Climatol.*, 49(5),
682 1044-1051.

683 Hong, Y., K. L. Hsu, X. Gao, and S. Sorooshian (2004), Precipitation estimation from remotely
684 sensed imagery using artificial neural network - cloud classification system
685 (PERSIANN-CCS), *J. Appl. Meteorol. Clim.*, 43(12), 1834–1853.

686 Hong, Y., R. F. Adler, F. Hossain, S. Curtis, and G. J. Huffman (2007), A first approach to global
687 runoff simulation using satellite rainfall estimation, *Water Resour. Res.*, 43(8), W08502, doi:
688 10.1029/2006WR005739.

689 Hossain, F., and D. P. Lettenmaier (2006), Flood prediction in the future: Recognizing hydrologic
690 issues in anticipation of the Global Precipitation Measurement mission, *Water Resour. Res.*,
691 42, W11301, doi:10.1029/2006WR005202.

692 Hou, Y. (2008), The Global Precipitation Measurement (GPM) mission: overview and U.S.
693 Science Status at the International Geoscience and Remote Sensing Symposium (IGARSS)
694 2008, *Invited Session 123: Global Precipitation Mission*, 6-11 July 2008, Boston, MA.

695 Huffman, G. J., R. F. Adler, D. T. Bolvin, and E. J. Nelkin (2010), The TRMM Multi-satellite
696 Precipitation Analysis (TMPA), *Satellite Applications for Surface Hydrology*, edited by F.

697 Hossain and M. Gebremichael, Springer, New York, 3-22.

698 Huffman, G. J., R. F. Adler, D. T. Bolvin, G. Gu, E. J. Nelkin, K. P. Bowman, Y. Hong, E. F.
699 Stocker, and D. B. Wolff (2007), The TRMM Multi-satellite Precipitation Analysis (TMPA):
700 Quasi-Global, Multi-Year, Combined-Sensor Precipitation Estimates at Fine Scales, *J.*
701 *Hydrometeo.*, 8, 38-55.

702 Huffman, G. J., R. F. Adler, M. Morrissey, D. T. Bolvin, S. Curtis, R. Joyce, B. McGavock, and J.
703 Susskind (2001), Global precipitation at one-degree daily resolution from multisatellite
704 observations, *J. Hydrometeo.*, 2, 36–50.

705 Joyce, R. J., J. E. Janowiak, P. A. Arkin, and P. Xie (2004), CMORPH: A method that produces
706 global precipitation estimates from passive microwave and infrared data at high spatial and
707 temporal resolution, *J. Hydrometeo.*, 5, 487-503.

708 Khan, S. I., Y. Hong, J. Wang, K.K. Yilmaz, J.J. Gourley, R.F. Adler, G.R. Brakenridge, F.
709 Policelli, S. Habib, and D. Irwin (2011), Satellite Remote Sensing and Hydrologic Modeling
710 for Flood Inundation Mapping in Lake Victoria Basin: Implications for Hydrologic
711 Prediction in Ungauged Basins, *IEEE Trans. Geosci. Remote Sens.*, 49(1), 85-95.

712 Kubota, T., and Coauthors (2007), Global precipitation map using satellite-borne microwave
713 radiometers by the GSMaP Project: Production and validation, *IEEE Trans. Geosci. Remote*
714 *Sens.*, 45, 2259-2275.

715 Kummerow, A. et al. (2000), The status of the Tropical Rainfall Measuring Mission (TRMM)
716 after two years in orbit. *J. Appl. Meteor.*, 39, 1965-1982.

717 Kummerow, C., W. S. Olson, and L. Giglio (1996), A simplified scheme for obtaining
718 precipitation and vertical hydrometeor profiles from passive microwave sensors, *IEEE Trans.*
719 *Geosci. Remote Sens.*, 34(5), 1213-1232.

720 Labow, G. J., J. R. Herman, L. -K. Huang, S. A. Lloyd, M. T. DeLand, W. Qin, J. Mao, and D. E.
721 Larko (2011), Diurnal variation of 340 nm Lambertian equivalent reflectivity due to clouds
722 and aerosols over land and oceans, *J. Geophys. Res.*, *116*, D11202,
723 doi:10.1029/2010JD014980.

724 Li, L., Y. Hong, J. Wang, R. F. Adler, F. S. Policelli, S. Habib, D. Irwn, T. Korme and L. Okello
725 (2009), Evaluation of the real-time TRMM-based multi-satellite precipitation analysis for an
726 operational flood prediction system in Nzoia Basin, Lake Victoria, Africa, *Nat. Hazards*, doi:
727 10.1007/s11069-008-9324-5.

728 Liang, X., D. P. Lettenmaier, E. F. Wood, and S. J. Burges (1994), A Simple hydrologically
729 Based Model of Land Surface Water and Energy Fluxes for GSMs, *J. Geophys. Res*, *99*(D7),
730 14415-14428.

731 Liang, X., E. F. Wood, and D. P. Lettenmaier (1996), Surface soil moisture parameterization of
732 the VIC-2L model: Evaluation and modification, *Glob. Planet. Change*, *13*, 195–206.

733 Maddox, R. A., J Zhang, J. J. Gourley, and K. W. Howard (2002), Weather radar coverage over
734 the contiguous United States, *Wea. Forecasting*, *17*, 927–934.

735 Margulis, S., and D. Entekhabi (2001), Temporal disaggregation of satellite-derived monthly
736 precipitation estimates and resulting propagation of error in partitioning of water at the land
737 surface, *Hydrol. Earth Syst. Sci.*, *5*(1), 27– 38.

738 Nikolopoulos, E. I., E. N. Anagnostou, F. Hossain, M. Gebremichael, and M. Borga (2010),
739 Understanding the scale relationships of uncertainty propagation of satellite rainfall through a
740 distributed hydrologic model, *J. Hydrometeorol.*, *11*, 520-532, doi: 10.1175/2009JHM1169.1.

741 Olson, W. S., C. D. Kummerow, Y. Hong, and W.-K. Tao (1999), Atmospheric Latent Heating
742 Distributions in the Tropics Derived from Satellite Passive Microwave Radiometer

743 Measurements, *J. Appl. Meteor. Climatol.*, 38(6), 633-664.

744 Serpetzoglou, E., E. N. Anagnostou, A. Papadopoulos, E. I. Nikolopoulos, and V. Maggioni
745 (2010), Error propagation of remote sensing rainfall estimates in soil moisture prediction from
746 a land surface model, *J. Hydrometeorol.*, 11, 705-702, doi: 10.1175/2009JHM1166.1.

747 Simpson, J., C. Kummerow, W. K. Tao, and R. F. Adler (1996), On the Tropical Rainfall
748 Measuring Mission (TRMM), *Meteorol. Atmos. Phys.*, 60, 19– 36.

749 Simpson, J., R. F. Adler, and G. R. North (1988), A proposed Tropical Rainfall Measuring
750 Mission (TRMM) satellite. *Bull. Amer. Meteor. Soc.*, 69, 278-295.

751 Smith, E., et al. (2006), The International Global Precipitation Measurement (GPM) program and
752 mission: An overview, in *Measuring Precipitation From Space: EURAINSAT and the Future*,
753 edited by V. Levizzani and F. J. Turk, Springer, New York, 28, 611-653.

754 Sorooshian, S. (2004), Commentary-GEWEX (Global Energy and Water Cycle Experiment) at
755 the 2004 Joint Scientific Committee Meeting, *GEWWX News*, 14(2), 2.

756 Sorooshian, S., K. L. Hsu, X. Gao, H. Gupta, B. Imam, and D. Braithwaite (2000), Evaluation of
757 PERSIANN system satellite-based estimates of tropical rainfall, *Bull. Amer. Meteor. Soc.*, 81,
758 2035-2046.

759 Steiner, M., T. L. Bell, Y. Zhang, and E. F. Wood (2003), Comparison of two methods for
760 estimating the sampling-related uncertainty of satellite rainfall averages based on a large radar
761 dataset, *J. Clim.*, 16, 3759–3778.

762 Su, F., H. Gao, G. J. Huffman, and D. P. Lettenmaier (2011), Potential Utility of the Real-Time
763 TMPA-RT Precipitation Estimates in Streamflow Prediction. *J. Hydrometeorol.*, 12, 444-455.

764 Su, F., J. C. Adam, L. C. Bowling, and D. P. Lettenmaier (2005), Streamflow simulations of the
765 terrestrial Arctic domain, *J. Geophys. Res.*, 110, D08112, doi:10.1029/2004JD005518.

766 Su, F., Y. Hong, and D. P. Lettenmaier (2008), Evaluation of TRMM Multi-satellite Precipitation
767 Analysis (TMPA) and its utility in hydrologic prediction in La Plata Basin, *J. Hydrometeo.*,
768 9(4),622-640.

769 Tapiador F. J., F. J. Turk, W. Petersen, A. Y. Hou, E. García-Ortega, L. A. T. Machado, C. F.
770 Angelis, P. Salio, C. Kidd, G. J. Huffman, M. Castro (2012), Global precipitation
771 measurement: Methods, datasets and applications. *Atmos. Res.*, 104-105: 70-97, doi:
772 10.1016/j.atmosres.2011.10.021.

773 Tian, Y., C. D. Peters-Lidard, B. J. Choudhury, and M. Garcia (2007), Multitemporal analysis of
774 TRMM-based satellite precipitation products for land data assimilation applications, *J.*
775 *Hydrometeo.*, 8, 1165-1183, doi: 10.1175/2007JHM859.1.

776 Tobin, K. J., and M. E. Bennett (2010), Adjusting Satellite Precipitation Data to Facilitate
777 Hydrologic Modeling, *J. Hydrometeorol.*, 11(4), 966-978.

778 Turk, F.J., and S.D. Miller (2005), Toward improving estimates of remotely-sensed precipitation
779 with MODIS/AMSR-E blended data techniques. *IEEE Trans. Geosci. Rem. Sensing*, 43,
780 1059-1069.

781 Turk, F. J., G. V. Mostovoy, and V.G. Anantharaj (2010), Soil moisture sensitivity to NRL-Blend
782 high-resolution precipitation products: analysis of simulations with two land surface models.
783 *IEEE J. Sel. Top. Appl. Earth Obs. Remote Sens.*, 3, 32-48.

784 Vicente, G. A., R. A. Scofield, and W. P. Menzel (1998), The operational GOES infrared rainfall
785 estimation technique. *Bull. Amer. Meteor. Soc.*, 79, 1883-1898.

786 Vila, D., R. Ferraro, and R. Joyce (2007), Evaluation and improvement of AMSU precipitation
787 retrievals, *J. Geophys. Res.*, 112, D20119, doi:10.1029/2007JD008617.

788 Wang, J., Y. Hong, J. J. Gourley, P. Adhikari, L. Li, and F. Su (2010), Quantitative assessment of

789 climate change and human impacts on long-term hydrologic response: a case study in a
790 sub-basin of the Yellow River, China. *Inter. J. Climatol.*, 30, 2130-2137, doi:
791 10.1002/joc.2023.

792 Wang, J., Y. Hong, L. Li, J. J. Gourley, K. Yilmaz, S. I. Khan, F. S. Policelli, R. F. Adler, S.
793 Habib, D. Irwn, S. A. Limaye, T. Korme, and L. Okello (2011), The Coupled Routing and
794 Excess STORAGE (CREST) distributed hydrological model, *Hydrol. Sciences Journal*, 56,
795 84-98.

796 Wilk, J., D. Kniveton, L. Andersson, R. Layberry, M. C. Todd, D. Hughes, S. Ringrose, and C.
797 Vanderpost (2006), Estimating rainfall and water balance over the Okavango River Basin for
798 hydrological application. *J. Hydrol.*, 331, 18–29.

799 Wu, H., R. F. Adler, Y. Hong, Y. Tian, and F. Policelli (2012), Evaluation of satellite-based
800 real-time global flood detection and prediction with a hydrological model. *J. Hydrometeorol.*
801 (In Press).

802 Yong, B., L. L. Ren, Y. Hong, J. H. Wang, J. J. Gourley, S. H. Jiang, X. Chen, and W. Wang
803 (2010), Hydrologic evaluation of Multisatellite Precipitation Analysis standard precipitation
804 products in basins beyond its inclined latitude band: A case study in Laohahe basin, China,
805 *Water Resour. Res.*, 46, W07542, doi:10.1029/2009WR008965.

806
807
808
809
810
811
812
813

814 **Table 1.** Time History of Major Upgrades of Microwave Satellites/Sensors Introduced into the
 815 TMPA Processing^a

Period	Satellites	Sensors	Period of Record	nominal coverage	Current Status
Period I	TRMM	TMI	8 Dec. 1997 – Current	40° N-S	Active
	TRMM	PR	8 Dec. 1997 – Current	38° N-S	Active
	DMSP-F13	SSM/I	29 Jan. 2002 – 18 Nov. 2009	85° N-S	Inactive
	DMSP-F14	SSM/I	29 Jan. 2002 – 23 Aug. 2008	85° N-S	Inactive
	DMSP-F15	SSM/I	29 Jan. 2002 – 14 Aug. 2006	85° N-S	Active, but unusable
Period II	Aqua	AMSR-E	3 Feb. 2005 – Current	85° N-S	Active
	NOAA-15	AMSU-B	3 Feb. 2005 – Current	Global	Active
	NOAA-16	AMSU-B	3 Feb. 2005 – Current	Global	Active
	NOAA-17	AMSU-B	3 Feb. 2005 – 17 Dec. 2009	Global	Inactive
	NOAA-18	MHS	27 Nov. 2007 – Current	Global	Active
Period III	MetOP-1	MHS	27 Mar. 2009 – Current	Global	Active
	DMSP-F16	SSMIS	Being incorporated into TMPA	85° N-S	Active
	DMSP-F17	SSMIS	Being incorporated into TMPA	85° N-S	Active

816

817 ^aNotation. Except for above microwave satellites/sensors, the international constellation of geosynchronous-orbit
 818 meteorological satellites including the Geosynchronous Operational Environmental Satellites (GOES, United
 819 States), the Geosynchronous Meteorological Satellite (GMS, Japan), and the Meteorological Satellite (Meteosat,
 820 European Community) provide the infrared (IR) data on a 4 km-equivalent grid over the latitude band 60° N-S for
 821 TMPA-RT.

822

823

824

825

826

827

828

829

Table 2. Statistical Summary of the Seasonal Comparison of Daily TMPA-RT vs. Gauge at Three Evolving Periods^a

Index	Evaluating domains	Spring									Summer									Autumn									Winter [Winter but excluding snowing days]								
		Period I			Period II			Period III			Period I			Period II			Period III			Period I			Period II			Period III			Period I			Period II			Period III		
CC	Grid 0501	0.16	0.47	0.63	0.38	0.47	0.68	0.36	0.39	0.53	0.02	0.03	0.03	0.03	0.08	0.15	0.03	0.08	0.15	0.03	0.08	0.15	0.03	0.08	0.15	0.03	0.08	0.15	0.03	0.08	0.15	0.03	0.08	0.15			
	Grid 0401	0.16	0.49	0.65	0.37	0.48	0.72	0.36	0.49	0.56	0.003	0.02	0.02	0.08	0.15	0.15	0.08	0.15	0.15	0.08	0.15	0.15	0.08	0.15	0.15	0.08	0.15	0.15	0.08	0.15	0.15	0.08	0.15	0.15			
	Basin Average	0.16	0.60	0.69	0.48	0.68	0.85	0.39	0.65	0.86	0.05	0.08	0.08	0.14	0.23	0.23	0.14	0.23	0.23	0.14	0.23	0.23	0.14	0.23	0.23	0.14	0.23	0.23	0.14	0.23	0.23	0.14	0.23	0.23			
ME (mm)	Grid 0501	1.05	1.38	0.90	1.48	1.29	3.51	1.77	0.97	0.31	1.19	0.55	0.31	0.64	0.35	1.39	0.64	0.35	1.39	0.64	0.35	1.39	0.64	0.35	1.39	0.64	0.35	1.39	0.64	0.35	1.39	0.64	0.35	1.39			
	Grid 0401	1.00	1.04	0.59	1.47	0.84	2.47	1.04	0.75	0.18	1.09	0.53	0.18	0.55	0.39	1.24	0.55	0.39	1.24	0.55	0.39	1.24	0.55	0.39	1.24	0.55	0.39	1.24	0.55	0.39	1.24	0.55	0.39	1.24			
	Basin Average	0.62	0.76	0.51	0.49	1.07	2.33	1.39	0.60	0.82	1.24	0.56	0.82	0.44	0.30	1.29	0.44	0.30	1.29	0.44	0.30	1.29	0.44	0.30	1.29	0.44	0.30	1.29	0.44	0.30	1.29	0.44	0.30	1.29			
RMSE (mm)	Grid 0501	6.00	4.39	4.28	12.28	7.79	11.89	7.77	3.72	3.45	3.98	1.89	3.45	2.13	1.28	5.80	2.13	1.28	5.80	2.13	1.28	5.80	2.13	1.28	5.80	2.13	1.28	5.80	2.13	1.28	5.80	2.13	1.28	5.80			
	Grid 0401	6.14	4.07	4.33	11.32	7.70	9.90	5.94	3.49	3.66	3.90	2.09	3.66	1.83	1.25	5.70	1.83	1.25	5.70	1.83	1.25	5.70	1.83	1.25	5.70	1.83	1.25	5.70	1.83	1.25	5.70	1.83	1.25	5.70			
	Basin Average	4.60	2.38	2.65	6.62	4.99	6.59	5.45	1.83	2.72	4.11	1.85	2.72	1.40	0.83	5.60	1.40	0.83	5.60	1.40	0.83	5.60	1.40	0.83	5.60	1.40	0.83	5.60	1.40	0.83	5.60	1.40	0.83	5.60			
BIAS (%)	Grid 0501	130.19	173.76	109.54	49.24	44.95	175.56	169.90	199.43	35.29	2104.65	1086.49	35.29	1399.94	751.89	1230.79	1399.94	751.89	1230.79	1399.94	751.89	1230.79	1399.94	751.89	1230.79	1399.94	751.89	1230.79	1399.94	751.89	1230.79	1399.94	751.89	1230.79			
	Grid 0401	134.89	133.91	66.29	48.32	26.61	108.80	84.60	141.65	18.61	1640.58	844.06	18.61	1357.14	11070.02	1096.01	1357.14	11070.02	1096.01	1357.14	11070.02	1096.01	1357.14	11070.02	1096.01	1357.14	11070.02	1096.01	1357.14	11070.02	1096.01	1357.14	11070.02	1096.01			
	Basin Average	85.39	106.35	59.09	46.52	36.71	106.58	135.06	118.10	35.89	1742.62	835.71	35.89	940.51	707.14	1300.39	940.51	707.14	1300.39	940.51	707.14	1300.39	940.51	707.14	1300.39	940.51	707.14	1300.39	940.51	707.14	1300.39	940.51	707.14	1300.39			
POD	Grid 0501	0.54	0.69	0.57	0.61	0.72	0.79	0.88	0.54	0.54	0.36	0.37	0.54	0.33	0.33	0.20	0.33	0.33	0.20	0.33	0.33	0.20	0.33	0.33	0.20	0.33	0.33	0.20	0.33	0.33	0.20	0.33	0.33	0.20			
	Grid 0401	0.50	0.61	0.54	0.60	0.71	0.81	0.74	0.60	0.64	0.20	0.21	0.64	0.25	0.33	0.50	0.25	0.33	0.50	0.25	0.33	0.50	0.25	0.33	0.50	0.25	0.33	0.50	0.25	0.33	0.50	0.25	0.33	0.50			
	Basin Average	0.56	0.77	0.64	0.66	0.86	0.92	0.84	0.83	0.90	0.50	0.33	0.90	0.33	0.50	0.33	0.33	0.50	0.33	0.33	0.50	0.33	0.33	0.50	0.33	0.33	0.50	0.33	0.33	0.50	0.33	0.33	0.50	0.33			
FAR	Grid 0501	0.84	0.82	0.69	0.36	0.38	0.37	0.60	0.69	0.68	0.94	0.95	0.68	0.98	0.96	0.97	0.98	0.96	0.97	0.98	0.96	0.97	0.98	0.96	0.97	0.98	0.96	0.97	0.98	0.96	0.97	0.98	0.96	0.97			
	Grid 0401	0.75	0.75	0.55	0.37	0.30	0.44	0.55	0.59	0.64	0.98	0.98	0.64	0.97	0.97	0.89	0.97	0.97	0.89	0.97	0.97	0.89	0.97	0.97	0.89	0.97	0.97	0.89	0.97	0.97	0.89	0.97	0.97	0.89			
	Basin Average	0.75	0.63	0.55	0.37	0.21	0.23	0.54	0.54	0.60	0.96	0.97	0.60	0.97	0.96	0.97	0.97	0.96	0.97	0.97	0.96	0.97	0.97	0.96	0.97	0.97	0.96	0.97	0.97	0.96	0.97	0.97	0.96	0.97			
CSI	Grid 0501	0.14	0.16	0.25	0.46	0.50	0.54	0.38	0.24	0.25	0.06	0.05	0.25	0.02	0.03	0.03	0.02	0.03	0.03	0.02	0.03	0.03	0.02	0.03	0.03	0.02	0.03	0.03	0.02	0.03	0.03	0.02	0.03	0.03			
	Grid 0401	0.20	0.22	0.33	0.45	0.55	0.49	0.39	0.32	0.30	0.02	0.02	0.30	0.03	0.03	0.10	0.03	0.03	0.10	0.03	0.03	0.10	0.03	0.03	0.10	0.03	0.03	0.10	0.03	0.03	0.10	0.03	0.03	0.10			
	Basin Average	0.21	0.33	0.36	0.48	0.70	0.72	0.43	0.42	0.38	0.04	0.03	0.38	0.03	0.04	0.03	0.03	0.04	0.03	0.03	0.04	0.03	0.03	0.04	0.03	0.03	0.04	0.03	0.03	0.04	0.03	0.03	0.04	0.03			
Error Contribution (EC)		20.73%									45.28%									18.94%									15.05%								

^aNotation. The seasonal comparison includes five cases: spring [March-May (MAM)], summer [June-August (JJA)], autumn [September-November (SON)], winter

[December-February (DJF)], and winter but excluding snowing days. The computing equation of Error Contribution (EC) is defined as:
$$EC = \frac{\sum_{i=1}^n |S_i - G_i|}{\sum_{j=1}^m |S_j - G_j|} \times 100\%$$

among which S_i and G_i are satellite precipitation and gauged observation, and n and m represent the number of a certain season and all season days, respectively.

Table 3. Number of Snowing Days, Observed Cumulative Snowmelt, and Statistical Indices (CC, ME, RMSE, and BIAS) of Daily TMPA-RT and TMPA-V6 vs. Gauge for Every Winter from 2005 to 2010 in Laohahe Basin^a

Phases	Year	Number of snowing days	Observed cumulative snowmelt	TMPA-RT vs. Gauge			TMPA-V6 vs. Gauge			Performance Level		
				CC	ME	RMSE	BIAS	CC	ME		RMSE	BIAS
Period II	2005	4	5.434	0.086	1.153	3.825	1909.40%	0.120	0.052	0.443	85.63%	Poor
	2006	4	4.766	-0.042	0.537	1.593	1013.50%	-0.009	0.014	0.381	26.56%	Average
	2007	2	3.400	0.249	0.388	1.232	1023.75%	0.539	0.029	0.273	75.19%	Average
	2008	3	3.480	0.237	0.409	1.319	1497.97%	0.218	0.061	0.393	221.84%	Average
Period III	2009	2	2.350	0.773	0.489	1.679	597.42%	0.888	0.085	0.313	104.31%	Good
	2010	5	10.540	-0.042	2.099	7.733	1791.94%	-0.045	0.076	0.857	64.99%	Poor

^aNotation. If the snowing observations of more than half rain gauges distributed within the whole basin exceed the threshold of 0.1mm, this day will be labeled as a “snowing day”.

861 **Table 4.** Comparison of Calibrated and Recalibrated Parameter Values in VIC-3L Hydrologic
 862 Model for TMPA-RT-driven Streamflow Simulations^a

Parameter	Unit	Typical Range	Calibrated values with gauge precipitation	Recalibrated values for TMPA-RT
b	N/A	0~0.5	0.01	0.0055
d_2	m	0.1~2.0	1.2	5.7
D_s	Fraction	0~1.0	0.004	0.0025
D_m	mm/day	0~30.0	8.0	7.3
W_s	Fraction	0~1.0	0.98	0.98
d_1	m	0~0.1	0.05	0.05
d_3	m	0.1~2.0	1.5	2.0

863

864 ^aNotation. In this study, the calibration period is Jan. 1990 - Dec. 1999 and the recalibration period is Feb. 2002 –
 865 Sep. 2010.

866

867

868

869

870

871

872

873

874

875

876

877

878

879

Table 5. Comparison Results of Rainfall-Runoff Error Propagation for Three Simulation Schemes, i.e., Validation, Bias-correction, and Recalibration through VIC-3L Hydrologic Model at Daily and Monthly Scales, Respectively

Item	Index	Daily scale									Monthly scale																										
		Period I			Period II			Period III			Period I			Period II			Period III																				
		Rainfall	Streamflow	Streamflow	Rainfall	Streamflow	Streamflow	Rainfall	Streamflow	Streamflow	Rainfall	Streamflow	Streamflow	Rainfall	Streamflow	Streamflow	Rainfall	Streamflow	Streamflow																		
Scheme 1: Validation	NSCE	-1.14	-161.62	0.01	-275.78	-2.05	-94.29	-0.35	-298.74	0.03	-348.21	-0.91	-205.08	0.46	0.02	0.70	0.24	0.67	-0.11	0.80	0.49	0.91	0.61	77.86	609.95	65.61	853.20	103.34	565.77	77.86	609.79	65.46	853.45	103.57	565.62		
	CC	5.29	385.27	3.10	482.12	4.72	298.07	46.95	48.09	30.19	59.90	51.50	38.33	0.02	-1.33	0.48	0.29	0.44	-1.44	0.62	0.47	0.79	0.67	0.46	0.23	0.70	0.55	0.63	0.67	0.18	0.80	0.71	0.91	0.85			
	BIAS (%)	0.00	23.78	0.00	13.60	0.00	5.75	0.00	23.76	0.00	13.60	0.00	5.78	0.00	23.78	0.00	13.60	0.00	23.76	0.00	13.60	0.00	5.78	0.00	23.78	0.00	13.60	0.00	13.60	0.00	13.60	0.00	13.60	0.00	13.60	0.00	13.60
	RMSE(mm)	3.57	46.05	2.26	22.93	1.92	25.14	30.18	4.34	23.04	2.34	18.30	1.53	0.44	-1.44	0.62	0.47	0.44	-1.44	0.62	0.47	0.79	0.67	0.46	0.23	0.70	0.55	0.63	0.67	0.18	0.80	0.71	0.91	0.85			
Scheme 2: Bias-correction	NSCE	-1.14	-0.45	0.01	0.32	-2.05	0.37	-0.35	-0.50	0.03	0.52	-0.91	0.61	0.46	0.34	0.70	0.57	0.67	0.32	0.80	0.76	0.91	0.85	77.86	-14.66	65.61	-6.30	103.34	7.52	77.86	-14.62	65.46	-6.33	103.57	7.58		
	CC	5.29	36.38	3.10	22.72	4.72	25.67	46.95	3.40	30.19	2.08	1.67	0.46	0.34	0.70	0.57	0.66	0.67	0.32	0.80	0.76	0.91	0.85	0.46	0.34	0.70	0.57	0.66	0.67	0.32	0.80	0.76	0.91	0.85			
	BIAS (%)	0.00	-14.66	65.61	-6.30	103.34	7.52	0.00	-14.62	65.46	-6.33	7.58	0.00	-14.62	65.46	-6.33	7.58	0.00	-14.62	65.46	-6.33	7.58	0.00	-14.62	65.46	-6.33	7.52	7.52	7.52	7.52	7.52	7.52	7.52	7.52	7.52		
	RMSE(mm)	3.57	36.38	3.10	22.72	4.72	25.67	46.95	3.40	30.19	2.08	1.67	0.46	0.34	0.70	0.57	0.66	0.67	0.32	0.80	0.76	0.91	0.85	0.46	0.34	0.70	0.57	0.66	0.67	0.32	0.80	0.76	0.91	0.85			
Scheme 3: Recalibration	NSCE	-1.14	-0.45	0.01	0.32	-2.05	0.37	-0.35	-0.50	0.03	0.52	-0.91	0.61	0.46	0.34	0.70	0.57	0.67	0.32	0.80	0.76	0.91	0.85	77.86	-14.66	65.61	-6.30	103.34	7.52	77.86	-14.62	65.46	-6.33	103.57	7.58		
	CC	5.29	36.38	3.10	22.72	4.72	25.67	46.95	3.40	30.19	2.08	1.67	0.46	0.34	0.70	0.57	0.66	0.67	0.32	0.80	0.76	0.91	0.85	0.46	0.34	0.70	0.57	0.66	0.67	0.32	0.80	0.76	0.91	0.85			
	BIAS (%)	0.00	-14.66	65.61	-6.30	103.34	7.52	0.00	-14.62	65.46	-6.33	7.58	0.00	-14.62	65.46	-6.33	7.58	0.00	-14.62	65.46	-6.33	7.58	0.00	-14.62	65.46	-6.33	7.52	7.52	7.52	7.52	7.52	7.52	7.52	7.52	7.52		
	RMSE(mm)	3.57	36.38	3.10	22.72	4.72	25.67	46.95	3.40	30.19	2.08	1.67	0.46	0.34	0.70	0.57	0.66	0.67	0.32	0.80	0.76	0.91	0.85	0.46	0.34	0.70	0.57	0.66	0.67	0.32	0.80	0.76	0.91	0.85			

882

883

884

885

886

887 **FIGURE CAPTIONS**

888 **Figure 1.** Map of Laohahe Basin situated beyond the TMI/PR orbiting bands (40°NS) and
889 locations of rain gauges, meteorological stations, and streamflow station included in the study.
890 Hydrologic evaluation of TMPA-RT during three major evolving periods was performed over the
891 whole basin (i.e., Basin Average) and two selected $0.25^{\circ}\times 0.25^{\circ}$ grids with black squares (i.e.,
892 Grid0501 and Grid0401), which contain 5 and 4 rain gauges, respectively.

893 **Figure 2.** Scatterplots of the daily TMPA-RT vs. gauge observation for (1st row) Grid 0501, (2nd
894 row) Grid 0401, and (3rd row) Basin Average at (left column) period I, (middle column) period II,
895 and (right column) period III.

896 **Figure 3.** Comparisons of statistical indices of the daily (left) TMPA-RT and (right) TMPA-V6
897 vs. gauge observation at three evolving periods (I-III): (a and b) correlation coefficient, (c and d)
898 mean error, and (e and f) relative bias, (g and h) probability of detection, (i and j) false alarm
899 ratio.

900 **Figure 4.** Monthly variations of gauged precipitation, TMPA-RT, and TMPA-V6 during three
901 evolving periods, i.e. Period I (Feb. 2002 – Jan. 2005), Period II (Feb. 2005 – Sep. 2008), and
902 Period III (Oct. 2008 – Sep. 2010): (a) Grid 0501, (b) Grid 0401, and (c) Basin Average.

903 **Figure 5.** Comparisons of gauge observation, TMPA-RT, and TMPA-V6 for two largest snowfall
904 events (i.e., 3 Jan. and 26 Feb.) in the winter of 2010 and two heavy rainstorms (i.e., 23-31 Jul.
905 and 17-22 Aug.) in the summer of 2010: (a and b) Grid 0501, (c and d) Grid 0401, and (e and f)
906 Basin Average.

907 **Figure 6.** Same as Figure 3 but for monthly precipitation: (a and b) correlation coefficient, (c and
908 d) mean error, and (e and f) relative bias.

909 **Figure 7.** Annual variations of statistical indices for daily TMPA-RT vs. TMPA-V6 over Grid
910 0501, Grid 0401, and Basin Average, respectively.

911 **Figure 8.** Same as Figure 7 but for seasonal statistics: (a) Spring [March-May (MAM)], (b)
912 Summer [June-August (JJA)], (c) Autumn [September-November (SON)], (d) Winter
913 [December-February (DJF)].

914 **Figure 9.** (a) Observed and gauge-driven VIC-simulated monthly streamflow for calibration
915 period (1990-1999) and reconstruction period (2000-2010), (b) Cumulative annual precipitation
916 from 1990 to 2010 for the Laohahe basin, (c) same as (b) but for streamflow.

917 **Figure 10.** Hydrologic simulation scheme 1: validation for TMPA-RT and TMPA-V6. VIC-3L
918 reconstructed streamflow with the observed gauge precipitation and VIC-3L simulated
919 streamflow directly forced by TMPA-RT and TMPA-V6 during three evolving periods: (a) daily
920 scale and (b) monthly scale.

921 **Figure 11.** Hydrologic simulation scheme 2: Simulation forced with bias-adjusted TMPA-RT.
922 Simulated streamflow with bias-adjusted TMPA-RT referenced by the reconstructed streamflow
923 with the gauged precipitation during three evolving periods: (a) daily scale and (b) monthly scale.

924 **Figure 12.** Hydrologic simulation scheme 3: recalibration for TMPA-RT. Recalibrated
925 streamflow with TMPA-RT (recalibrated model parameter values listed in Table 4) referenced by
926 the reconstructed streamflow with the gauged precipitation during three evolving periods: (a)
927 daily scale and (b) monthly scale.

928

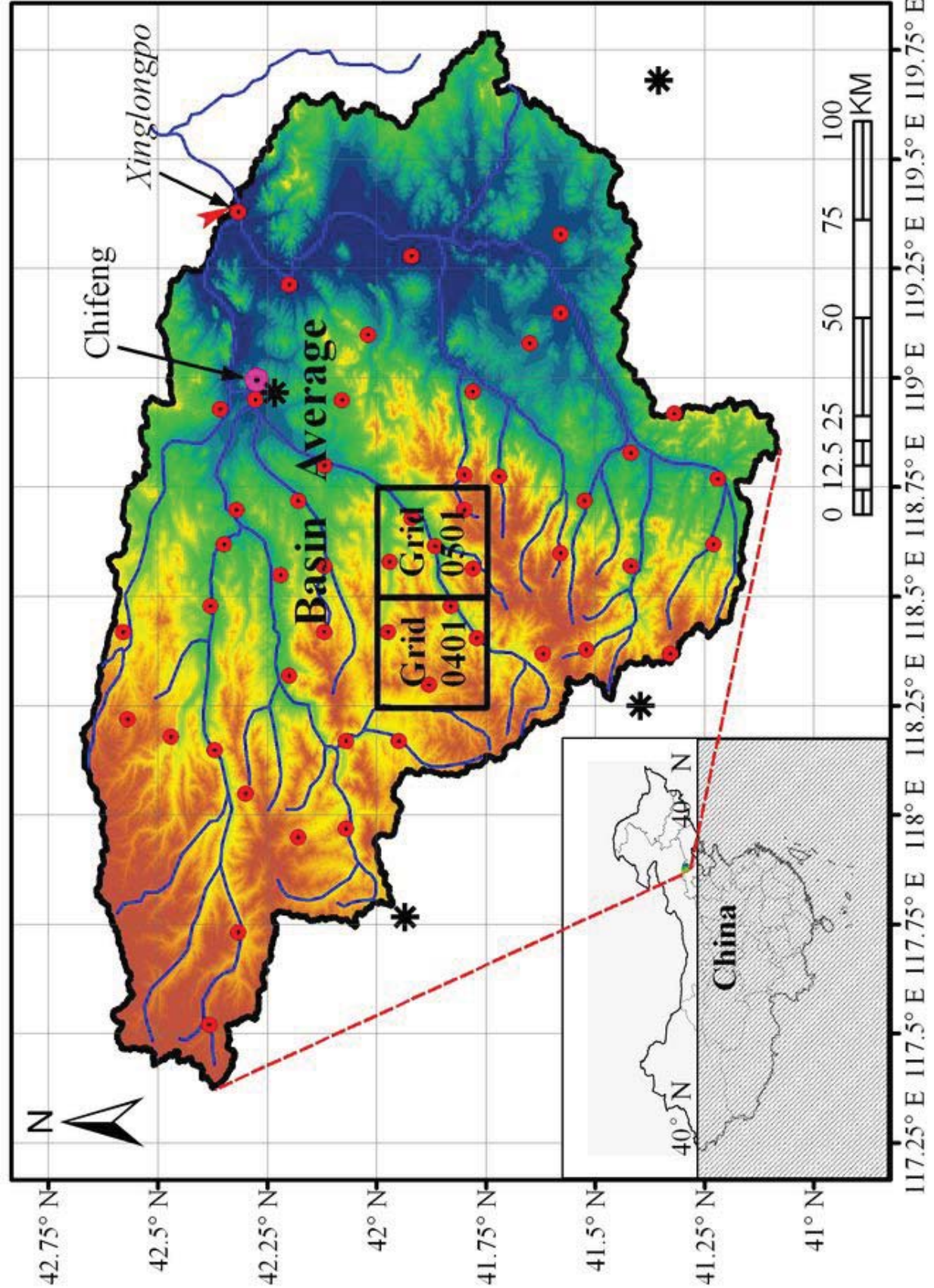
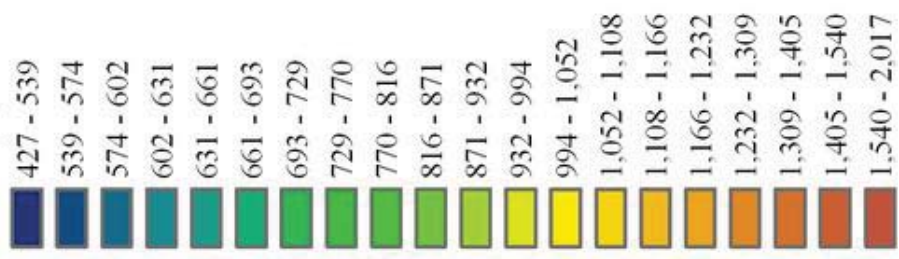
Laohahe Basin

Legend

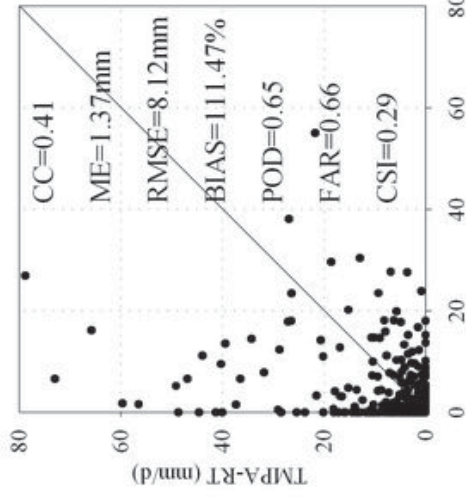
- Rainfall Gauge
- ✱ Meteorological Station
- ▶ Streamflow Station
- Chifeng City
- River
- Basin Boundary

- Basin Boundary
- Chifeng City
- River

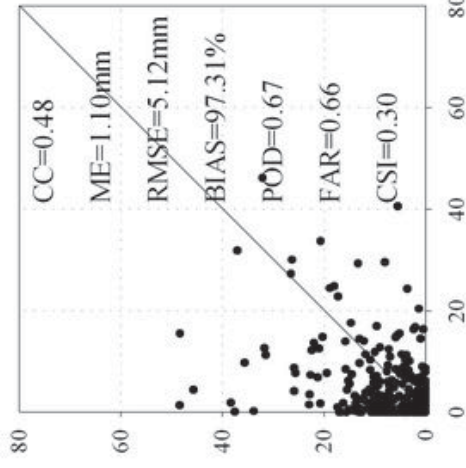
DEM (m)



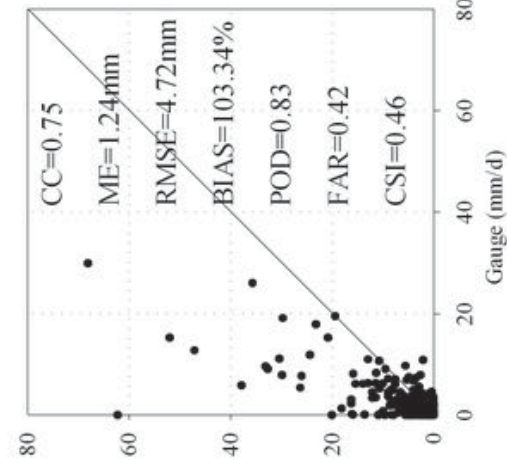
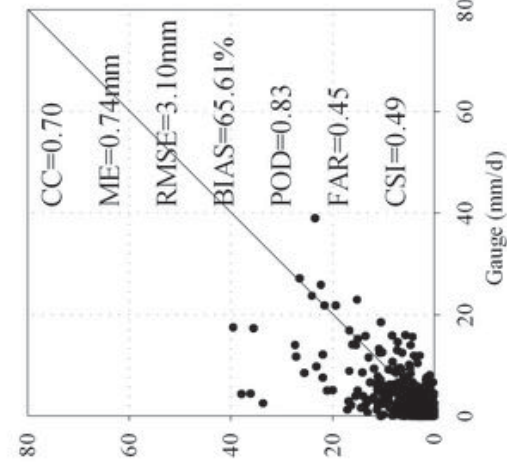
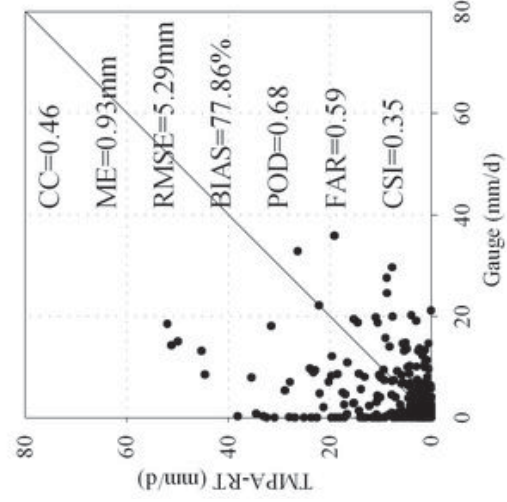
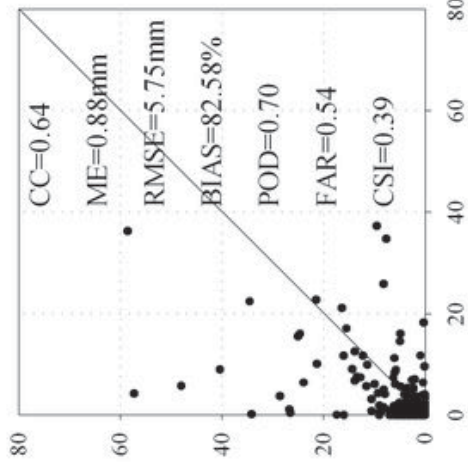
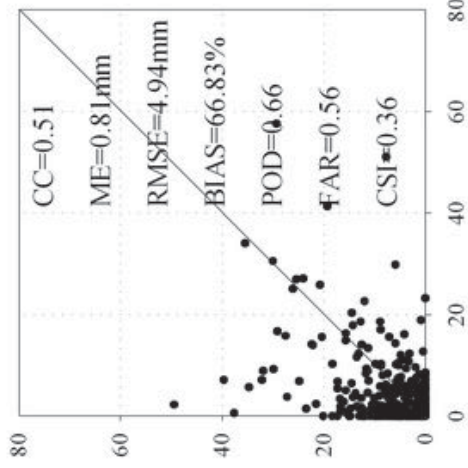
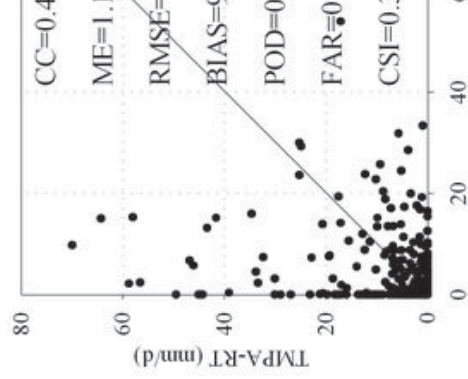
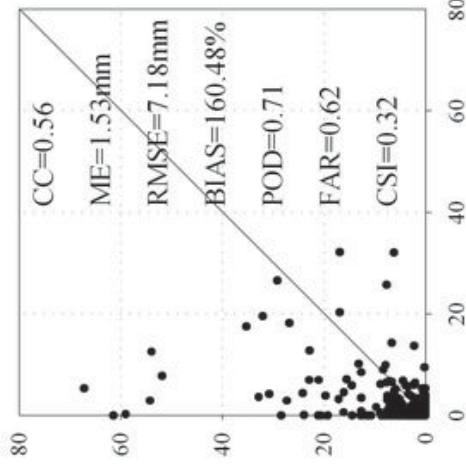
Period I



Period II

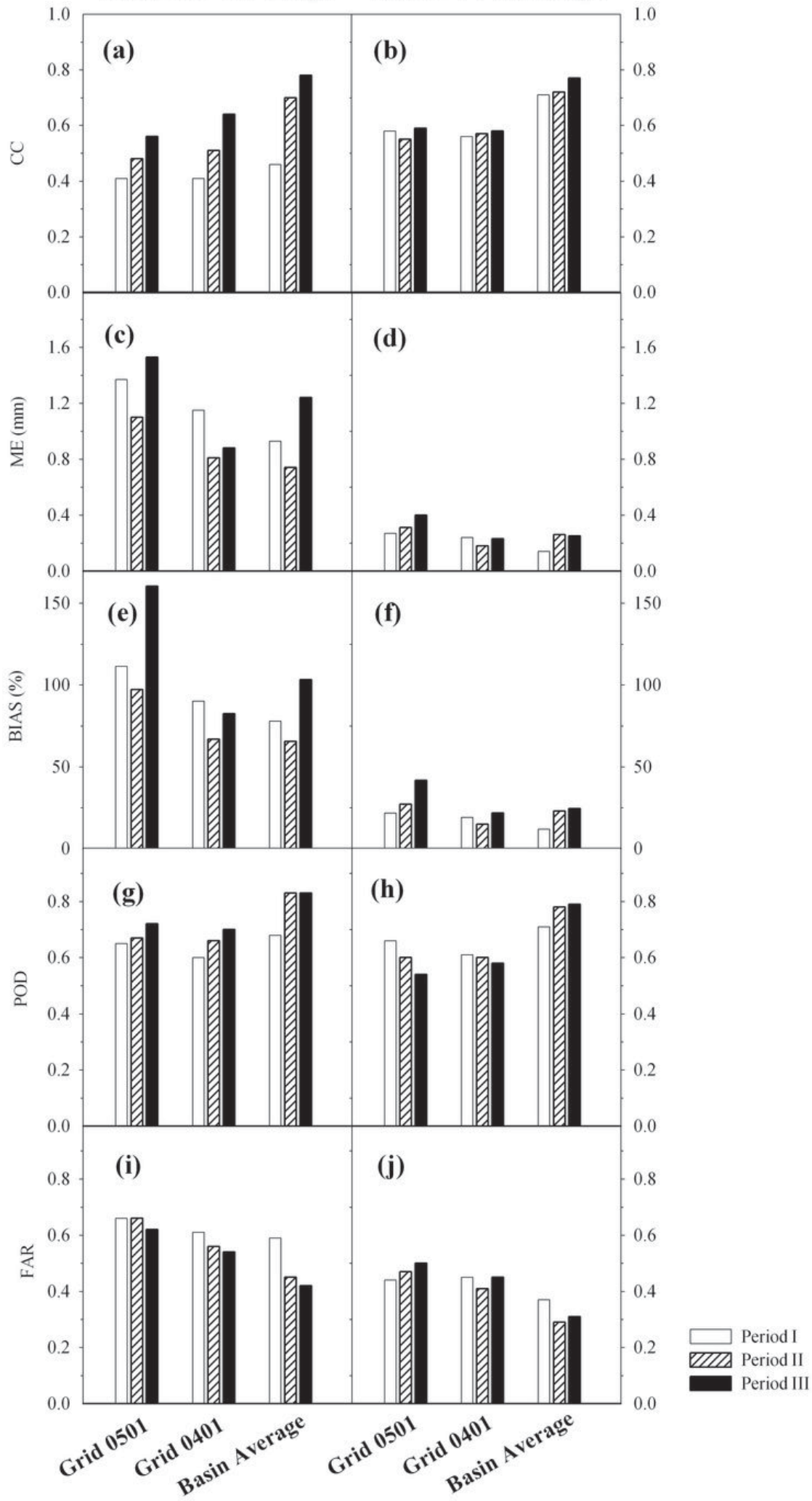


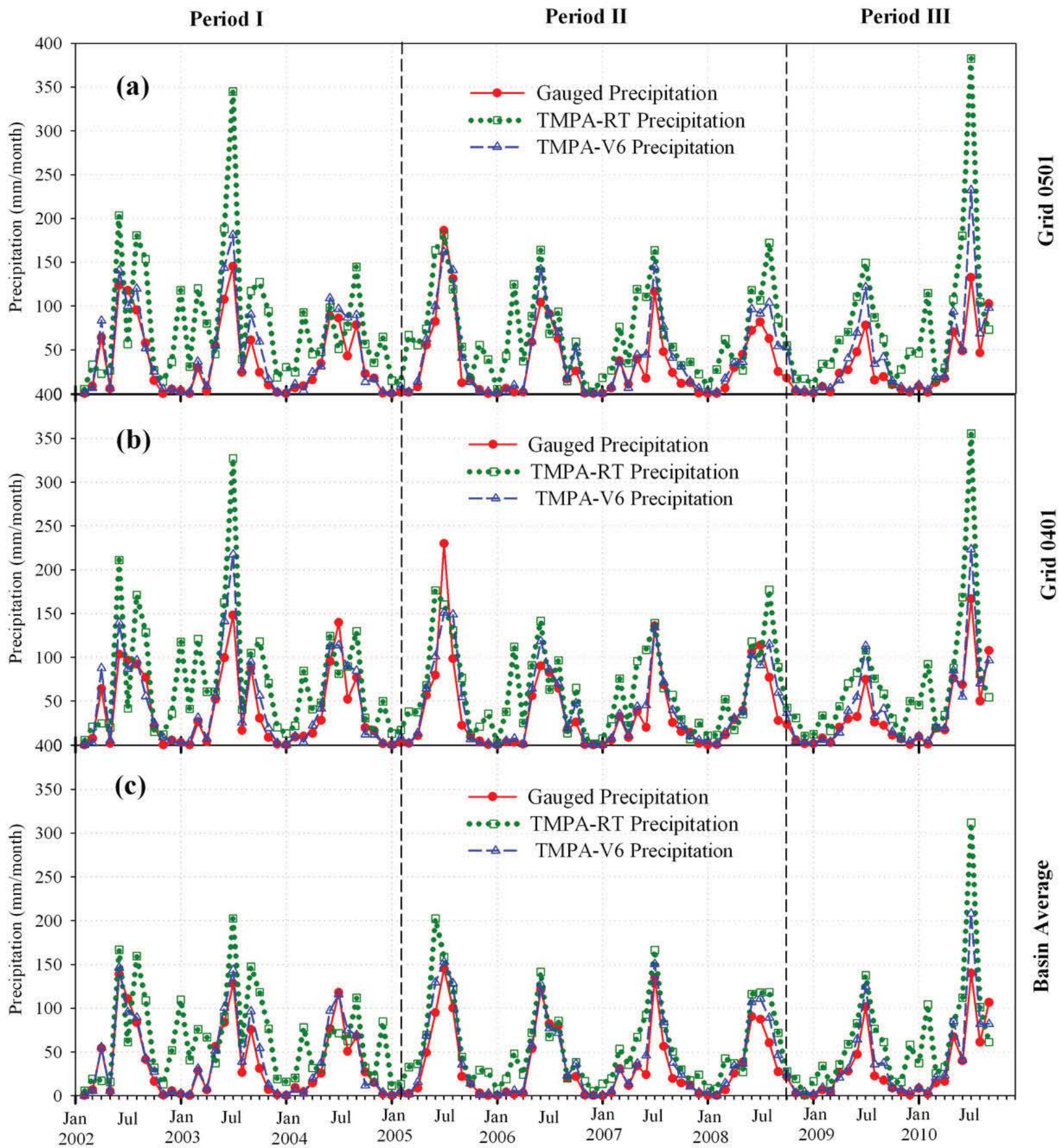
Period III



TMPA-RT vs. Gauge

TMPA-V6 vs. Gauge





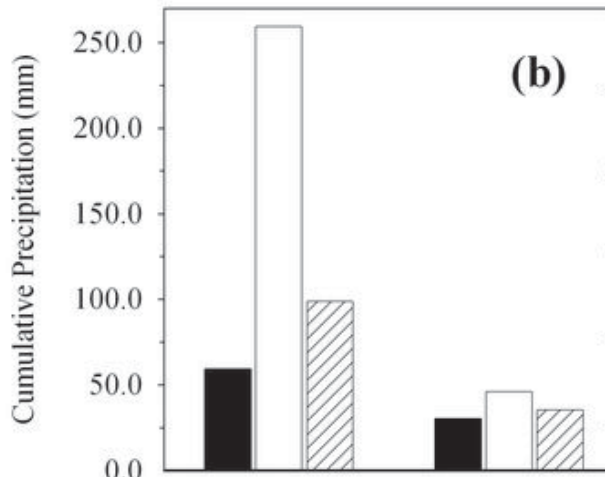
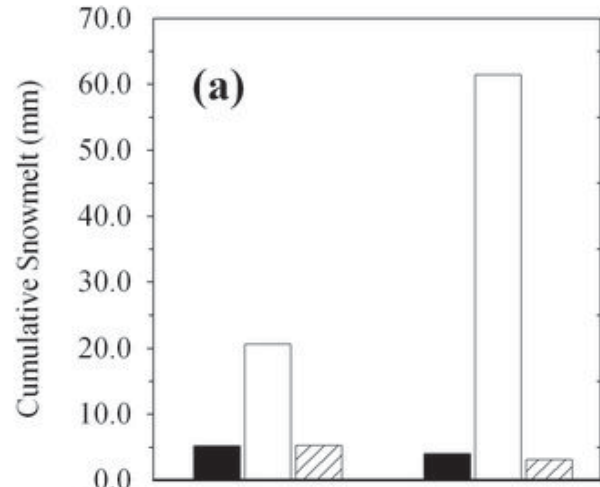
Grid 0501

Grid 0401

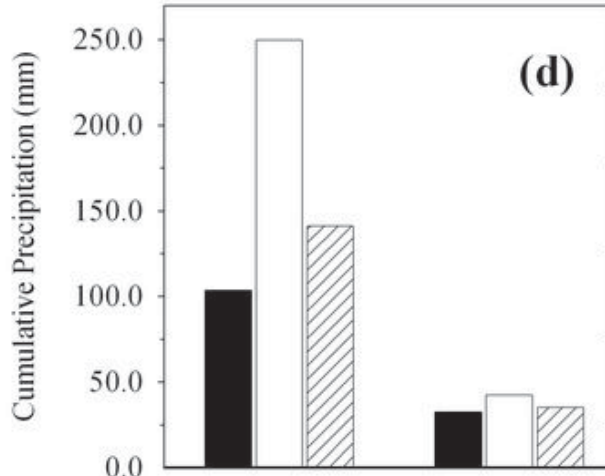
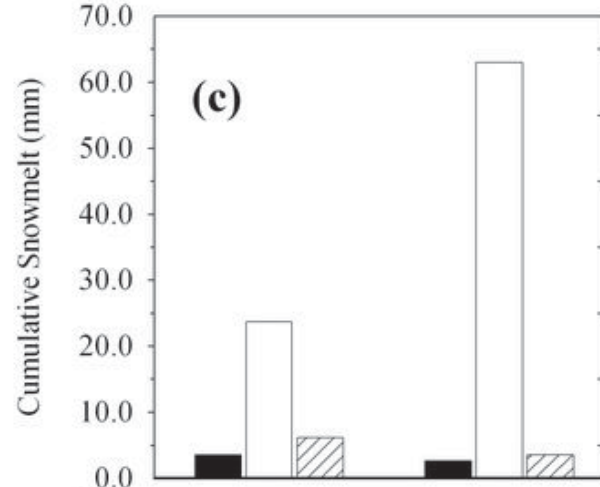
Basin Average

Two Largest Snowfall Events

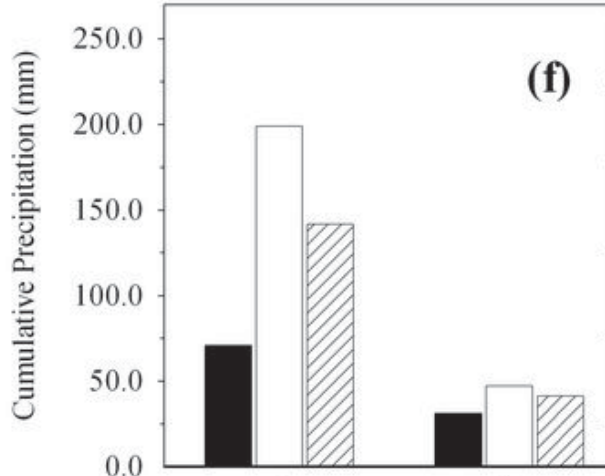
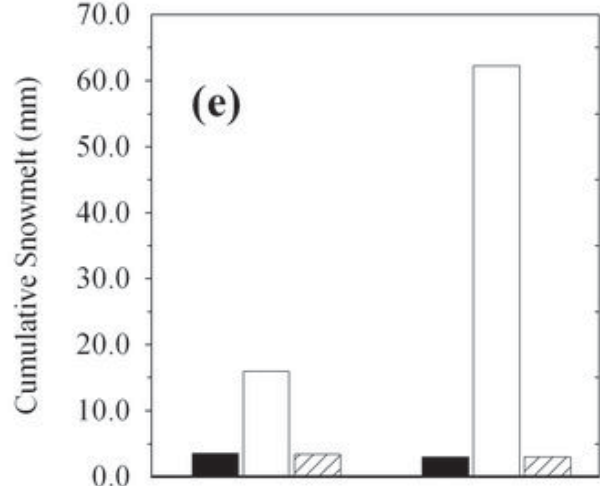
Two Largest Rainstorm Events



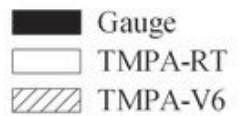
Grid 0501



Grid 0401



Basin Average



3 Jan. 2010

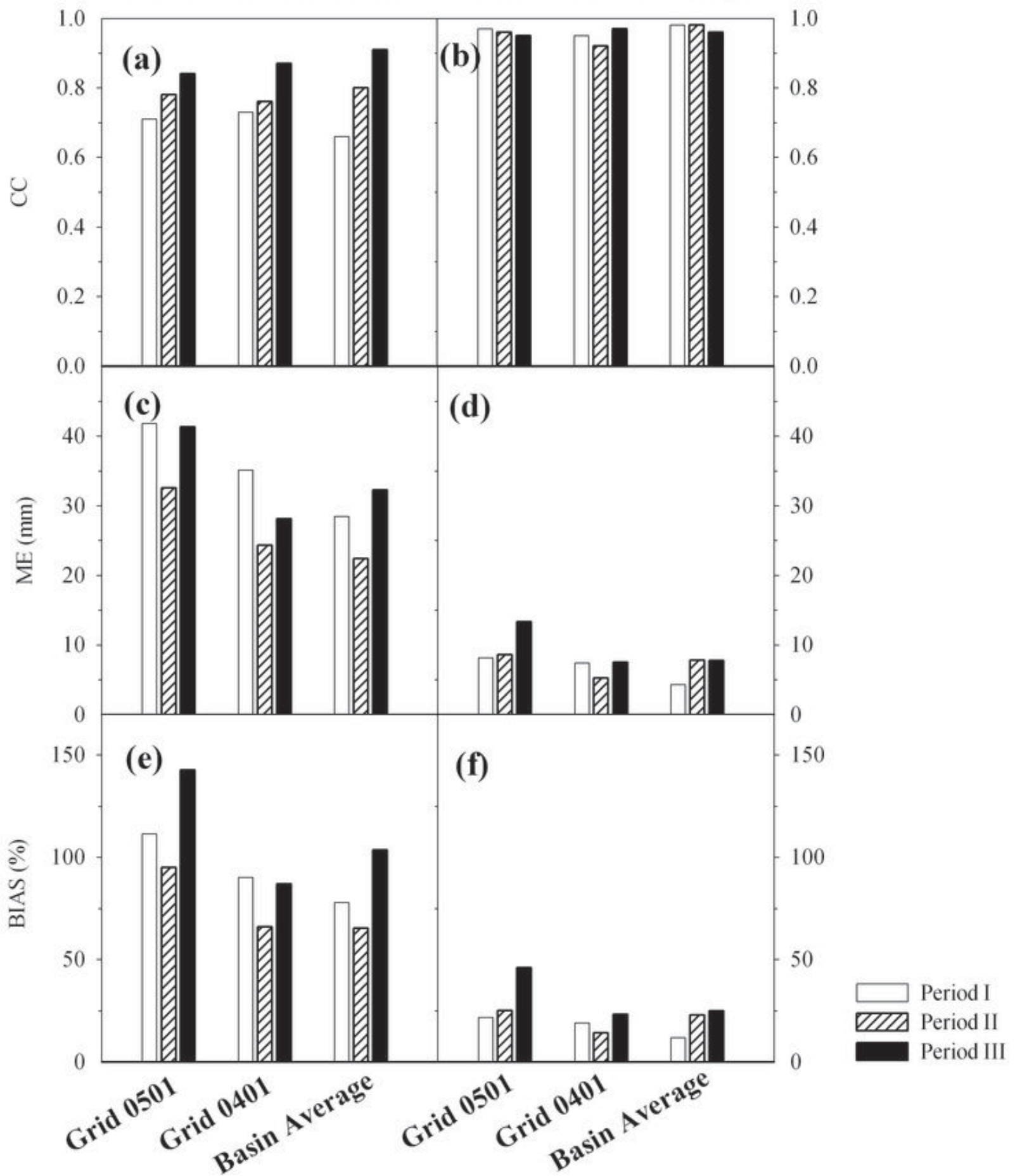
26 Feb. 2010

23~31 Jul. 2010

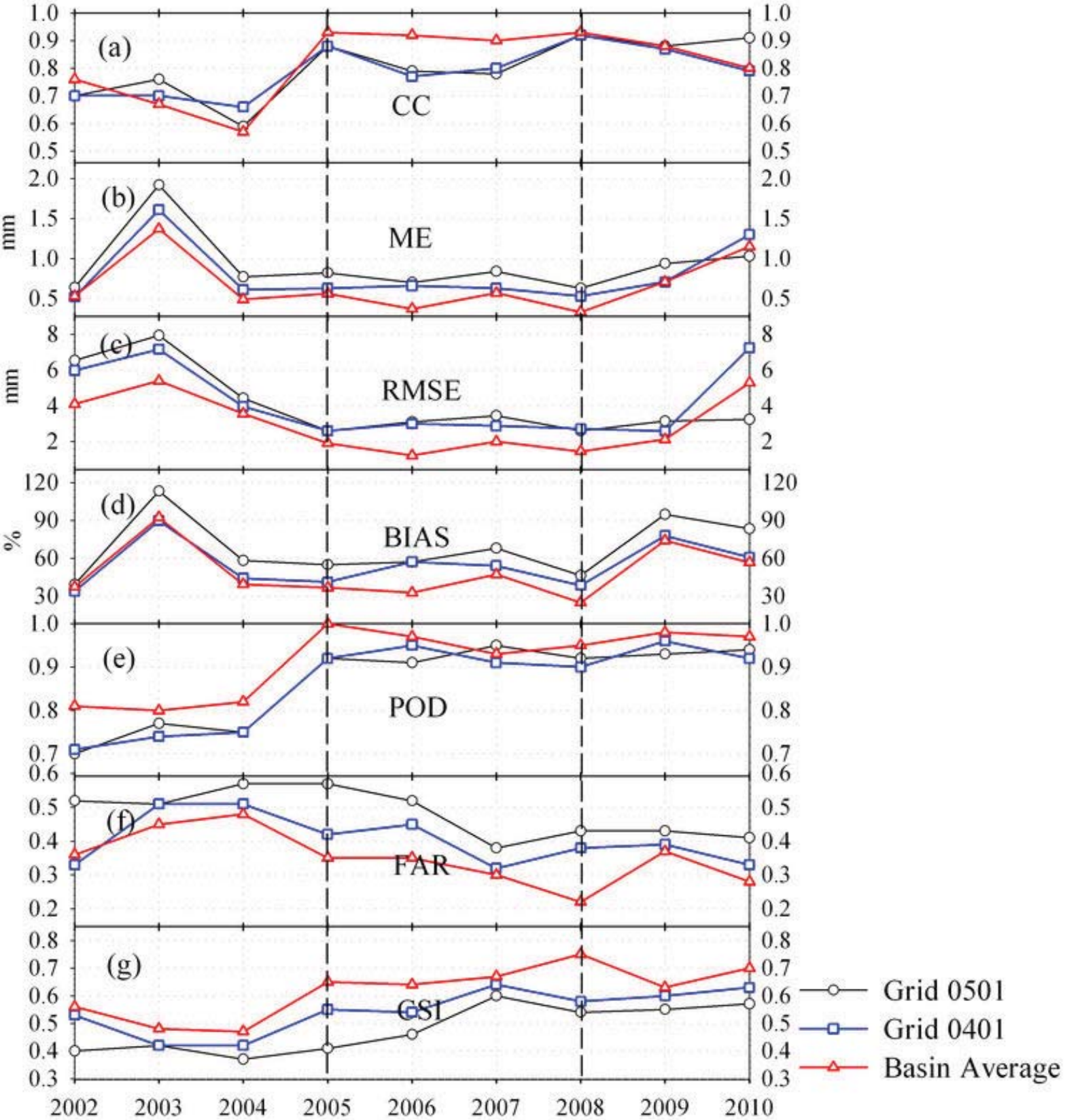
17-22 Aug. 2010

TMPA-RT vs. Gauge

TMPA-V6 vs. Gauge

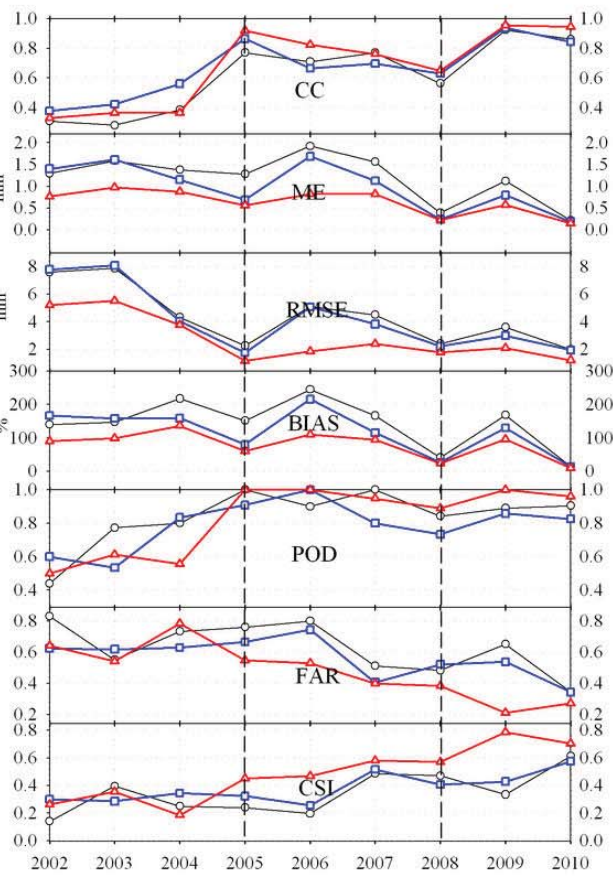


Period I Period II Period III

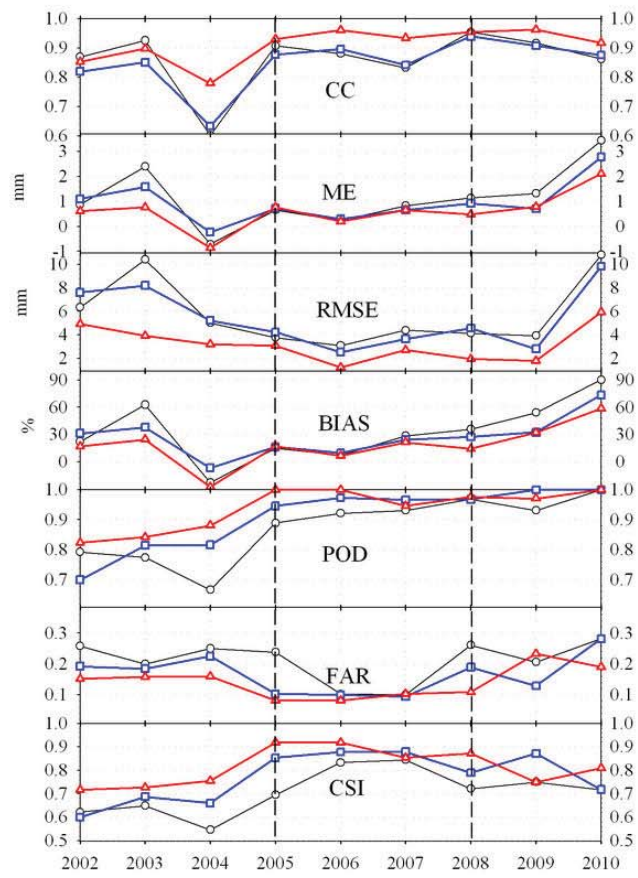


○ Grid 0501
 □ Grid 0401
 ▲ Basin Average

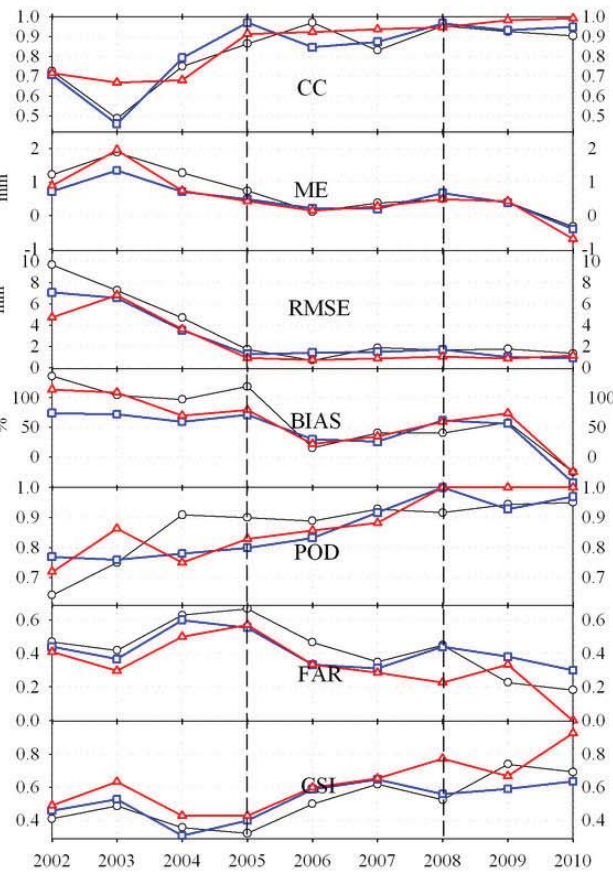
(a) Period I Period II Period III



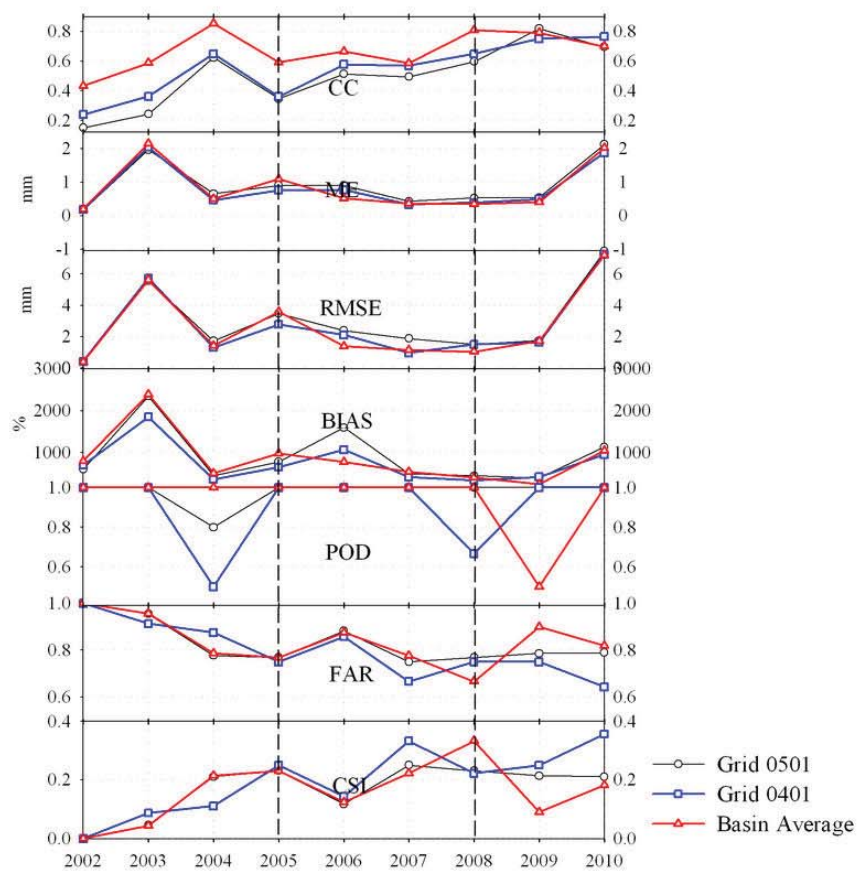
(b) Period I Period II Period III



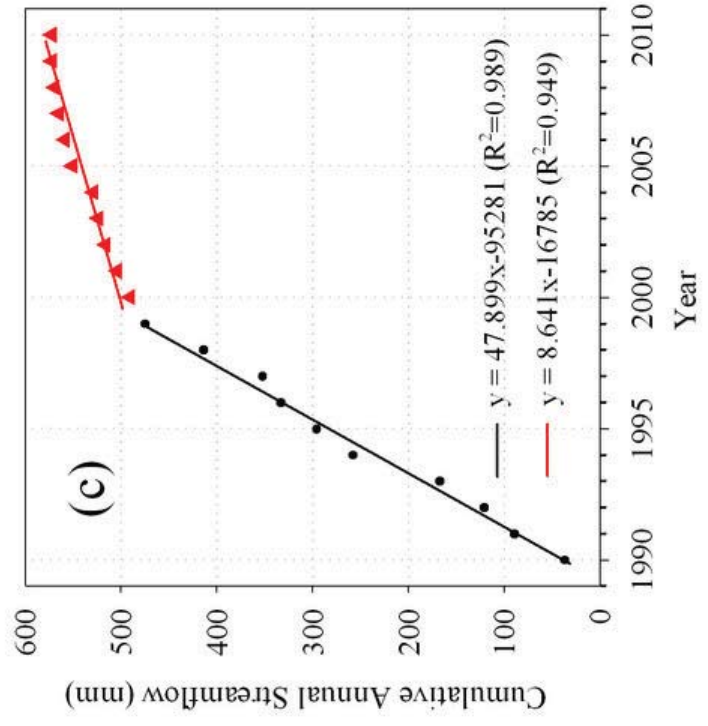
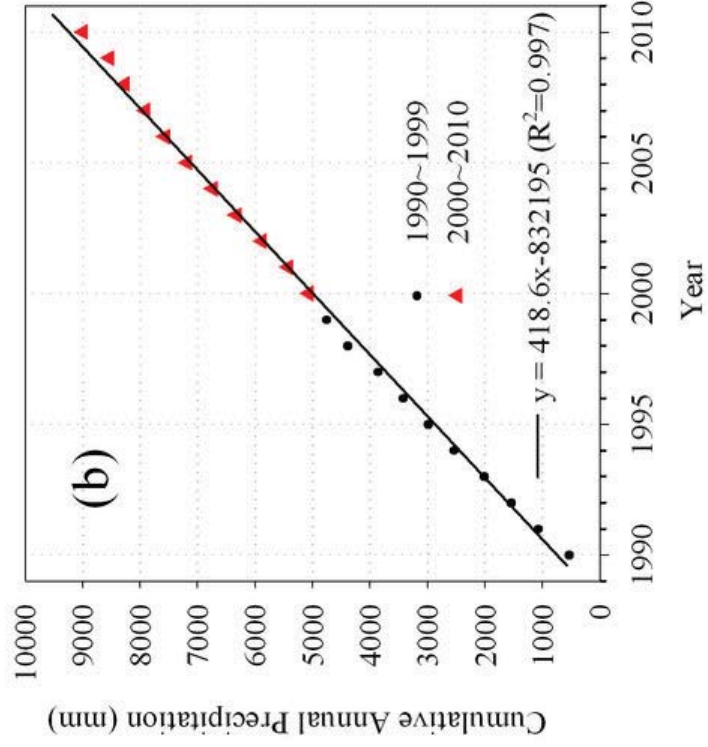
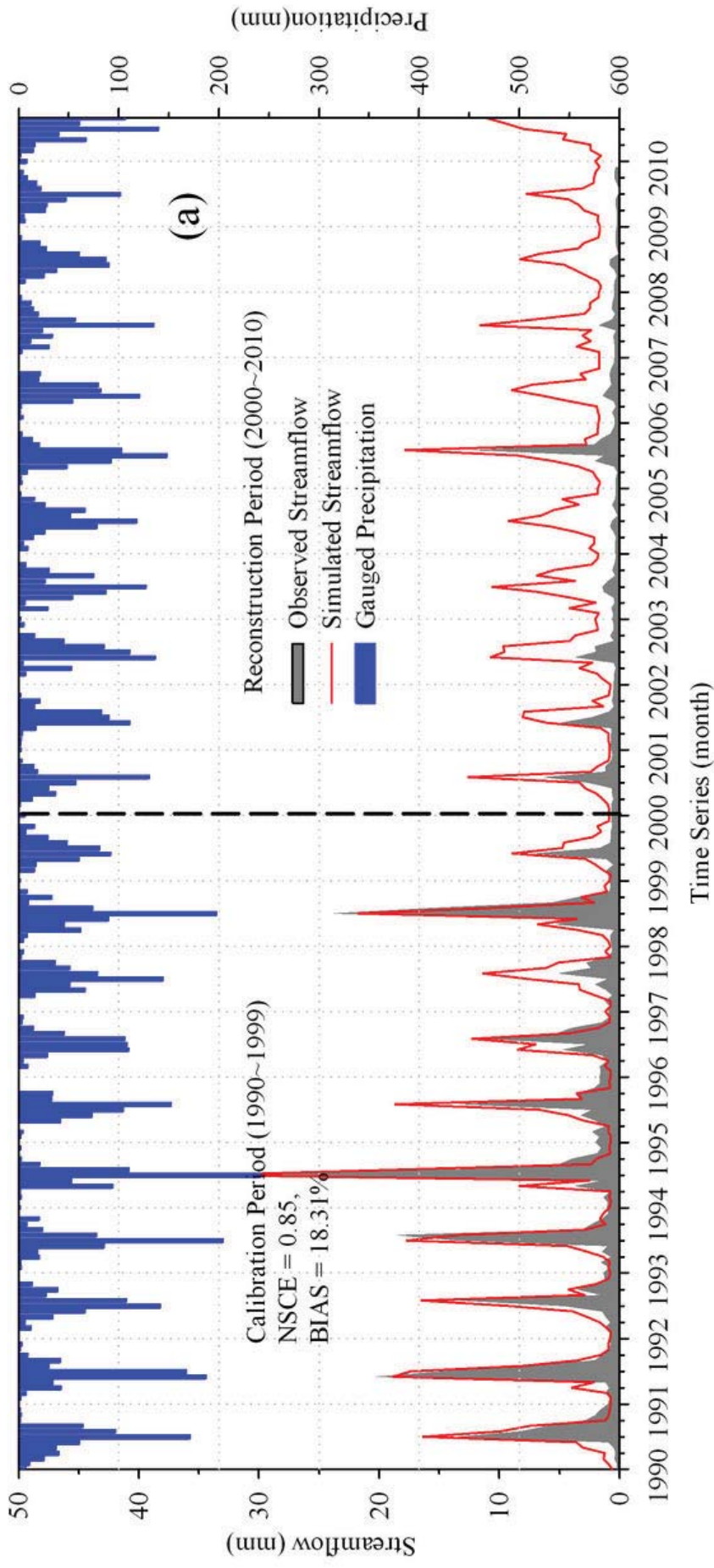
(c) Period I Period II Period III

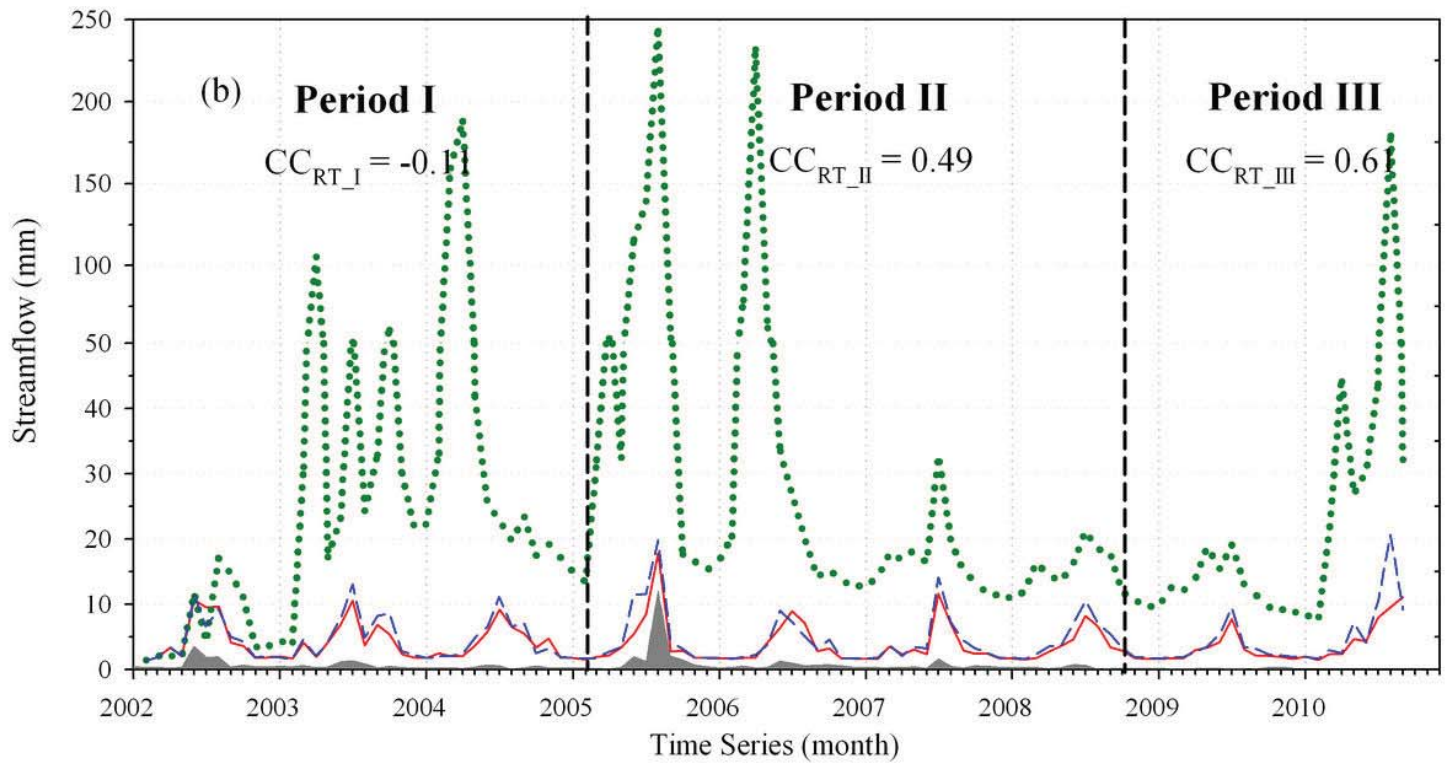
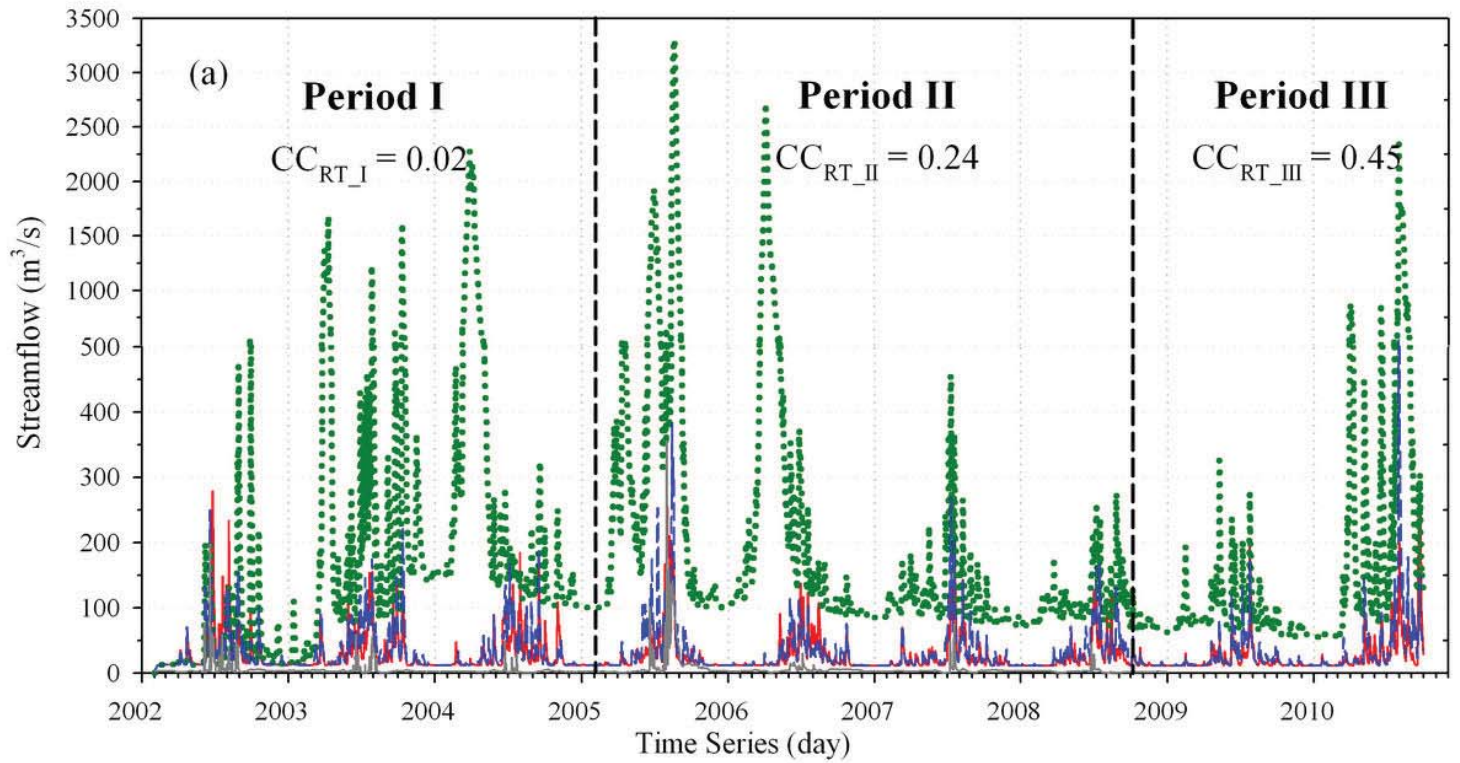


(d) Period I Period II Period III



○ Grid 0501
□ Grid 0401
△ Basin Average





Observed Streamflow
 Reconstructed with Gauged Data

Simulated with TMPA-RT
 Simulated with TMPA-V6

